

Oxygen-Bearing Functionalities Enhancing NO₂, NH₃, and Acetone Electronic Response and Response Variation by Polythiophenes in Organic Field-Effect Transistor Sensors

Justine Wagner^a, Yunjia Song^a, Jenna Shapiro^b, and Howard E. Katz^{a*}

^aDepartment of Materials Science and Engineering, Johns Hopkins University, 206 Maryland Hall, 3400 North Charles Street, Baltimore, MD 21218. ^bAnn & Robert H. Lurie Children's Hospital of Chicago, Pritzker Department of Psychiatry and Behavioral Health, Northwestern University Feinberg School of Medicine, Department of Psychiatry and Behavioral Sciences

*Corresponding author: email hekatz@jhu.edu

Supporting Information

Methods

Materials and characterization techniques

Unless otherwise specified, all chemicals were used as purchased without further purification. Solvents used for workups and cleaning were reagent grade and used as received.

¹H NMR spectra (Appendix B1-28) were measured on a Bruker Avance 300 MHz Spectrometer and chemical shifts are reported in parts per million (ppm). Spectra were recorded in either CDCl₃ or DMSO-d₆. Gel permeation chromatography (GPC) analysis was used to determine molecular weight (Appendix B29-32). The analysis was performed on a Tosoh Bioscience EcoSEC GPC workstation using THF as the eluent (0.35 mL min⁻¹), 40°C through a TSKgel SuperMultipore HZ-M guard column (4.6 mm ID x 2.0 cm, 4 mm, Tosoh Bioscience). Polystyrene standard (EasiVial PS-M, Agilent) was used to build a calibration curve. P3HT polymer and copolymers were dissolved in THF (2 mg mL⁻¹), filtered (Millex-FG Syringe Filter Unit, 0.20 mm, PTFE, EMD Millipore) and injected using an auto-sampler (10 µL). The same

procedure was performed for OTBS protected polythiophene but unfortunately polymers were insoluble in THF when protecting group was cleaved to form hydroxyl terminated ends.

NO₂ (49 ppm molar concentration) balanced with nitrogen and NH₃ (51 ppm) balanced with nitrogen were purchased from Praxair. The air/gas mixture with ranging controlled diluted concentrations, obtained by an Environics 4040 series gas dilution system, was introduced into the sealed probe chamber under continuous flow. The balanced air was purified by flowing through a series of purification stages of silica gel, carbon black, deoxy-catalyst, and Purafil to obtain clean air with minimum contamination of other gases that may hinder or alter measurements. The devices were exposed to each subset of gas concentrations for a total of 3 minutes before measuring. These diluted gases were further diluted before sample measurement, and exhausted into a well-ventilated open space to avoid reaching exposure limits for these toxic gases. Acetone (1012 ppm molar concentration) balanced with nitrogen was purchased from Airgas.

Field effect characteristics of the devices were determined using a Keysight 1500A Semiconductor Device Analyzer. The mobility of the OFETs in the saturation regime was extracted from the following equation:

$$I_D = \frac{W}{2L} \mu C_i (V_g - V_{TH})^2;$$

where I_D is the drain current that is collected; L and W are the channel length and width, respectively; μ is the mobility of the OFET; C_i is the gate capacitance per unit area; V_G is the gate voltage applied, and V_{TH} is the threshold voltage. The V_{TH} of the device was determined by

extrapolating the intercept of the x-axis of the $(I_{D,sat})^{1/2}$ vs. V_G plot. All measurements were measured in ambient environment conditions.

Conductivity measurements were performed by using a four- point probe measurement method with an Agilent 4155C Semiconductor Parameter Analyzer. At least six measurements of resistance were measured on each sample surface. The same positions were remeasured when exposing the surface to gas for a time duration of 20 minutes.

Fabrication of devices

The architecture of the gas sensing device is based on a bottom-gate, top-contact OFET structure with a semiconducting polymer serving as the organic active layer. The OFET was fabricated according to the process outlined below. A heavily doped p-type Si wafer and a layer of dry oxidized SiO_2 (300 nm) were used as a gate electrode and gate dielectric layer, respectively. The wafer was successively cleaned in an ultrasonicated bath with isopropanol for 15 minutes each. These substrates were then further purified by immersion in a piranha solution (2 : 1 mixture of sulfuric acid and 30% hydrogen peroxide – CAUTION- STRONGLY OXIDIZING AND CORROSIVE!) overnight. This was followed by rinsing with distilled water and drying under nitrogen flow. For the active organic layer consisting of either P3HT or P3HT-copolymers, the wafer was exposed to ultraviolet-ozone for 30 minutes. The stock solutions of the polymers were made by dissolving P3HT or P3HT-copolymers (10 mg mL^{-1}) in anhydrous chlorobenzene. The solutions were then ultrasonicated for 1 hour before placing on a hot bath at $60 \text{ }^\circ\text{C}$ for additional hour. When cooling to room temperature, the polymer solutions were filtered using a hydrophobic PTFE 0.45 mm membrane. The PTOH polymer and PTOH-copolymers were dissolved in anhydrous DMF (10 mg mL^{-1}), ultrasonicated for 1 h, and placed

on a hot bath at 60°C for 1 h before increasing the temperature to 130°C for 15 minutes and removing the solution to cool at room temperature. The solution, after cooling, was then filtered using a hydrophilic PTFE 0.45 mm membrane. The P3HT and P3HT-copolymer solutions were then deposited onto the respective clean wafer substrates via a 1-step spin coating process at 1600 rpm for 60 seconds, while PTOH and PTOH-copolymers were deposited at 1600 rpm for 320 seconds. The substrates coated with the thin organic films were baked at 60°C overnight in a glovebox to outgas any residual solvent present. Film thicknesses were measured with a Filmetrics F20-NIR, thin film analyzer. Finally, the OFET was completed by the addition of the source and drain electrodes by depositing 50 nm of gold via thermal evaporation using a shadow mask. The length and width of the active channel were 200 mm and 8 mm, respectively. The evaporation rate was maintained between 0.3–0.4 Å s⁻¹ under a chamber pressure of 3 x 10⁻⁶ Pa.

Silicon FET detection using remote gate

The RG active film was processed similarly to the above without the addition of the deposited gold source and drain electrodes. The polymer solutions were each individually deposited onto their own respective 1 in. x 1 in. Si/SiO₂ (300 nm oxide growth) substrates. After thoroughly out-gassing overnight at 60°C on a hot plate, the substrates with polymers deposited on them were diced into 1 in. x 0.5 in. slices. The FET detection system platform is divided into two components: a commercial Si FET (CD4007UB) and a RG module. A scratch was made to expose the Si surface on the polymer/SiO₂/Si substrate and the exposed Si is used as the electrode and electrically coupled to the gate of the FET. A drop (20 mL) of acetonitrile (ACN) was placed as the contact between the thin film surface and a dual Ag/AgCl (saturated

KCl) reference electrode to apply a gate bias. The surface potential variation on the RG module would transfer to the commercial FET and induce a horizontal shift of the transfer curve (V_{TH} shift) that is measured. A shift toward depletion, making the n-FET easier to turn on, would correspond to increased positive potential on the RG. Before exposure to the designated gas concentration, the surface potential was equilibrated between the RG and FET using ACN which would eventually reach a stabilization point where successive scans would overlay and obtain a finalized V_{TH} . The solvent drop was then removed, and the RG modules were exposed to 1 ppm NO_2 or NH_3 for 20 minutes, reconnected to the FET platform, had the drop reapplied, and remeasured for 20 consecutive scans to analyze drift and restoration. The procedure was repeated with 20 ppm NO_2 exposure. To evaluate recovery and restoration of initial V_{TH} , the remote gate substrates were subjected to a vacuum oven set at 60°C for 1 h. The same process outlined above occurred with a pristine sample that would be subjected to NH_3 exposure.

Materials.

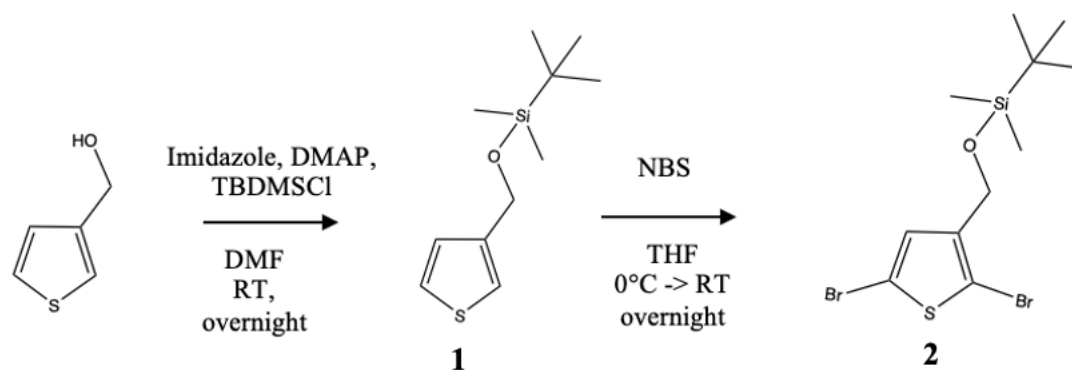
Polymer Synthesis and Characterization.

All polymer reactions were performed under air-free conditions using standard Schlenk techniques. All glassware was dried overnight at 110°C oven setting. N-Bromosuccinimide ($\geq 99\%$) and Triphenylphosphine ($\geq 99\%$) was purchased from Chem-Impex International.

Anhydrous Dimethylformamide, anhydrous Tetrahydrofuran, Sodium Hydride (60% dispersion in mineral oil), Imidazole (ACS reagent), 4-(Dimethylamino)pyridine (ReagentPlus), tert-Butyldimethylsilyl chloride (reagent grade, 97%), Copper Chromite, Quinoline (reagent grade, 98%), Isopropylmagnesium Chloride (2.0 M in THF), Lithium Chloride ($\geq 99\%$ trace metals basis), and Tetrabutylammonium Fluoride Solution (1.0 M in THF) were purchased from Sigma

Aldrich. Triethylene Glycol 2-Bromoethyl Methyl Ether (>95%), 1-Bromo-2-(2-methoxyethoxy)ethane (stabilized with Na₂CO₃, >90%), 3-Thiophenemethanol (>96%), Diethylene Glycol (> 99.5%), Triethylene Glycol (> 99.0%), Dimethyl 3,4-dihydroxy-2,5-thiophenedicarboxylate (>98.0%), and [1,3-Bis(diphenylphosphino)propane]nickel (II) Dichloride (>98%) were purchased from TCI. Diisopropyl Azodicarboxylate (94%) was purchased from Alfa Aesar. Potassium Hydroxide (Pellets, Certified ACS), Hydrochloric Acid (Certified ACS Plus, 36.5-38%), Diethyl Ether (BHT stabilized), Ethyl Acetate (ACS reagent), Hexanes (ACS reagent), Sodium Chloride (Crystalline, Certified ACS), Sodium Sulfate (Granular, Certified ACS), Acetone (ACS reagent), Methanol (ACS reagent), and Chloroform (ACS reagent) were purchased from Fisher Scientific.

Monomer Synthesis:



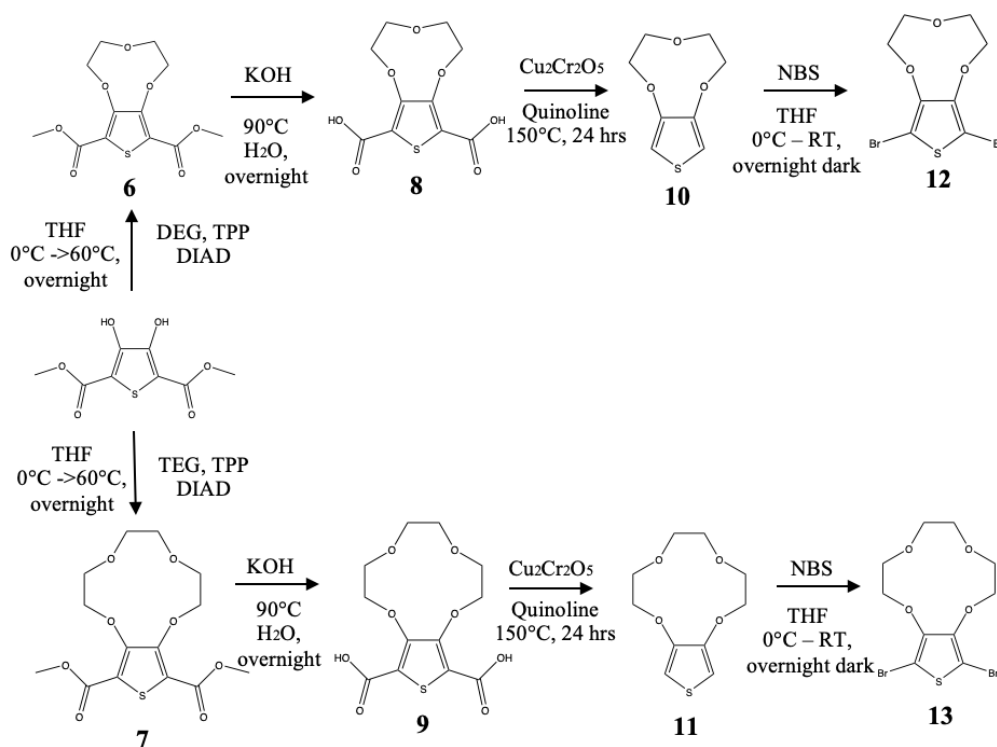
Scheme S1. Synthesis of OTBS functionalized thiophene monomer

- 1) **Tert-butyldimethyl(thiophen-3-ylmethoxy)silane:** In a round bottom flask charged with a stir bar was added 3-thiophenemethanol (2.50 g, 21.9 mmols, 1 eq.) dissolved in

50 mL of anhydrous DMF. Imidazole (3.73 g, 54.7 mmols, 2.5 eq.) and DMAP (134 mg, 1.1 mmols, 0.05 eq.) was added. The solution mixed at room temperature for 10 minutes before tert-butyldimethylsilyl chloride (3.96 g, 26.3 mmols, 1.2 eq.) was added. The mixture was left to stir at room temperature overnight. Afterwards, the mixture was concentrated in vacuo, redissolved in ethyl acetate and washed with water (x3) and brine (x1). All organic layers were collected, dried over with sodium sulfate, filtered, and concentrated in vacuo. The crude product was purified by silica gel column chromatography using (20:80) Diethyl Ether: Hexanes as elutant ($R_f = 0.8$). (78% yield, clear oil).

- 2) **Tert-butyl(2,5-dibromothiophen-3-ylmethoxy)dimethylsilane.** In a round bottom flask charged with a stir bar was added N-bromosuccinimide (4.88 g, 27.4 mmols, 2.5 eq.). The reaction vessel was purged with argon for 15 minutes before 50 mL of anhydrous THF was added. The reaction was placed on an ice bath at 0°C before tert-butyldimethyl(thiophen-3-ylmethoxy)silane (2.50 g, 10.96 mmols, 1 eq.) was slowly added. The reaction mixture stirred for 0°C for 1 hour before the ice bath was removed and the mixture continued to stir at room temperature overnight with no exposure to light. Afterwards, the mixture was concentrated in vacuo, redissolved in diethyl ether, and washed with water (x3) and brine (x1). All organic layers were collected, dried over with sodium sulfate, filtered, and concentrated in vacuo. The crude product was purified by using silica gel chromatography using 100% hexanes as the elutant ($R_f=0.5$) to receive a slightly yellow oil (85%).

- 4) **2,5-dibromo-3-((2-(2-methoxyethoxy)ethoxy)methyl)thiophene:** In a round bottom flask charged with a stir bar was added (2,5-dibromothiophen-3-yl)methanol (2.69 g, 9.9 mmols, 1 eq.) Then 50 mL of anhydrous DMF was added followed by slow addition of NaH (285 mg, 11.9 mmols, 1.5 eq.) The reaction was left to stir over an hour before slow addition of 1-Bromo-2-(2-methoxyethoxy)ethane (2.17 g, 11.9 mmols, 1.2 eq.). The reaction then placed on an oil bath at 50°C and left to stir overnight. Afterwards, the mixture was concentrated in vacuo upon complete dryness and purified by loading onto a silica gel column using (1:4) EtOAc : Hexanes to receive a clear yellow oil.
- 5) **2,5-dibromo-3-(2-(2-(2-(2-methoxyethoxy)ethoxy)ethoxy)ethyl)thiophene:** In a round bottom flask charged with a stir bar was added (2,5-dibromothiophen-3-yl)methanol (200 g, 7.4 mmols, 1 eq.) Then 50 mL of anhydrous DMF was added followed by slow addition of NaH (270 mg, 11.0 mmols, 1.5 eq.) The reaction was left to stir over an hour before slow addition of Triethylene glycol 2-bromoethyl methyl ether (2.40 g, 8.8 mmols, 1.2 eq.). The reaction then placed on an oil bath at 50°C and left to stir overnight. Afterwards, the mixture was concentrated in vacuo upon complete dryness and purified by loading onto a silica gel column using (1:1) EtOAc : Hexanes to receive a clear yellow oil.



Scheme S3. Synthesis of crown ether functionalized thiophene monomers

- 6) **Dimethyl 2,3,5,6-tetrahydrothieno[3,4-b][1,4,7]trioxonine-8.10-dicarboxylate [3-crown-dicarboxylate-thiophene]:** To a 3-neck round bottom flask charged with a stir bar was added dimethyl 3,4-dihydroxy-2,5-thiophenedicarboxylate (0.250 mg, 1.08 mmols, 1 eq.), diethylene glycol (102 μ L, 1.08 mmols, 1 eq.), and triphenylphosphine (564 mg, 2.15 mmols, 2 eq.) dissolved in 15 mL of anhydrous THF under an argon atmosphere. The reaction vessel was then placed on an ice bath at 0°C before slowly adding by drop wise addition a solution of DIAD (508 μ L, 2.59 mmols, 2.4 eq.) dissolved in additional anhydrous THF (5 mL). After stirring on an ice bath at 0°C for 1 hour, the reaction was placed on an oil bath at 60°C and stirred overnight. Afterwards, the reaction was removed and cooled to room temperature before concentrating in

vacuo, redissolved in diethyl ether, TPPO was filtered off, and reconcentrated in vacuo. The process occurred a few times to remove as much TPPO. Purification of the crude product occurred by silica gel chromatography by using (1:1) Hexanes: EtOAc as the elutant which afforded product as a white crystal solid ($R_f = 0.5$).

7) Dimethyl 2,3,5,6-tetrahydrothieno[3,4-b][1,4,7]trioxonine-8.10-dicarboxylic acid [3-crown-dicarboxylic acid-thiophene]: To a round bottom flask was charged dimethyl 2,3,5,6-tetrahydrothieno[3,4-b][1,4,7]trioxonine-8.10-dicarboxylic acid [3-crown-dicarboxylic acid-thiophene] (0.500 g, 1.65 mmols, 1 eq.) which was suspended in a solution of KOH (387 mg, 6.90 mmols, 4.17 eq.) in distilled water. The reaction was then placed on an oil bath at 90°C and left to stir overnight. Afterwards, the solution was left to cool at room temperature before it was slowly acidified with 1 M HCl. The solution was left to stir before a visible greyish white precipitate formed. The product was filtered, washed with water, and then dried under a vacuum oven at 60°C overnight (90% yield).

8) 2,3,5,6-tetrahydrothieno[3,4-b][1,4,7]trioxonine [3-crown thiophene]: To a round bottom flask was added dimethyl 2,3,5,6-tetrahydrothieno[3,4-b][1,4,7]trioxonine-8.10-dicarboxylic acid (0.500 mg, 1.82 mmols, 1 eq.) and copper chromite (136 mg, 0.44 mmols, 0.24 eq.). The vessel was evacuated from air and recharged with argon (this cycle process was done 3 times before backfilling with argon). Afterwards, 10 mL of quinoline was added and the reaction was wrapped with aluminum foil and left to stir at 150°C for a full day. Afterwards, the reaction was left to cool at room temperature and

then poured into a 1 M HCl solution. The product was extracted out of the 1M HCl solution with diethyl ether, washed with distilled water, and then brine. The diethyl ether fraction was collected, dried over with sodium sulfate, filtered, and concentrated under vacuum. The crude product was purified by column chromatography using (3:4) Hexanes: EtOAc to afford a yellow liquid (90% yield).

9) 2,5-dibromo-2,3,5,6-tetrahydroethieno[3,4-b][1,4,7]trioxonine: In a round bottom flask charged with a stir bar was added N-bromosuccinimide (1.26 g, 7.10 mmols, 2.1 eq.) The reaction vessel was purged with Argon for 15 minutes before 50 mL of anhydrous THF was added and sealed completely. The reaction was placed on an ice bath at 0°C for 1 hour before 2,3,5,6-tetrahydroethieno[3,4-b][1,4,7]trioxonine (0.628 g, 3.37 mmols, 1 eq.) was slowly added the ice bath was removed and left to continue to stir at room temperature overnight in the dark. Afterwards, the reaction was concentrated in vacuo, redissolved in diethyl ether, and washed with water (x3) and brine (x1). The organic layers were collected, dried over with sodium sulfate, filtered, and concentrated in vacuo. The crude product was purified by silica gel column chromatography using (1:1) EtOAc: Hexanes as elutant to receive a gray powder.

10) Dimethyl 2,3,5,6,8,9-hexahydrothienol[3,4-b][1,4,7,10]tetraoxacyclododecine-11,13, dicarboxylate [4-crown-dicarboxylate-thiophene]: To a 3-neck round bottom flask charged with a stir bar was added dimethyl 3,4-dihydroxy-2,5-thiophenedicarboxylate (0.250 mg, 1.08 mmols, 1 eq.), triethylene glycol (144 µL, 1.08 mmols, 1 eq.), and triphenylphosphine (564 mg, 2.15 mmols, 2 eq.) dissolved in 15 mL of anhydrous THF

under an argon atmosphere. The reaction vessel was then placed on an ice bath at 0°C before slowly adding by drop wise addition a solution of DIAD (508µL, 2.59 mmols, 2.4 eq.) dissolved in additional anhydrous THF (5 mL). After stirring on an ice bath at 0°C for 1 hour, the reaction was placed on an oil bath at 60°C and stirred overnight. Afterwards, the reaction was removed and cooled to room temperature before concentrating in vacuo, redissolved in diethyl ether, TPPO was filtered off, and reconcentrated in vacuo. The process occurred a few times to remove as much TPPO. Purification of the crude product occurred by silica gel chromatography by using (1:1) Hexanes: EtOAc as the elutant which afforded product as a white crystal solid ($R_f = 0.4$) (60% yield).

11) Dimethyl 2,3,5,6,8,9-hexahydrothienol[3,4-b][1,4,7,10]tetraoxacyclododecine-11,13, dicarboxylic acid [4-crown-dicarboxylic acid-thiophene]: To a round bottom flask was charged dimethyl 2,3,5,6,8,9-hexahydrothienol[3,4-b][1,4,7,10]tetraoxacyclododecine-11,13, dicarboxylic acid [4-crown-dicarboxylic acid-thiophene] (0.826 g, 2.38 mmols, 1 eq.) which was suspended in a solution of KOH (558 mg, 9.94 mmoles, 4.17 eq.) in distilled water. The reaction was then placed on an oil bath at 90°C and left to stir overnight. Afterwards, the solution was left to cool at room temperature before it was slowly acidified with 1 M HCl. The solution was left to stir before a visible greyish white precipitate formed. The product was filtered, washed with water, and then dried under a vacuum oven at 60°C overnight (100% yield).

12) 2,3,5,6,8,9-hexahydrothienol[3,4-b][1,4,7,10]tetraoxacyclododecine [4-crown thiophene]:

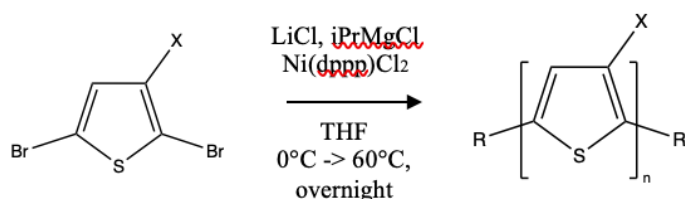
To a round bottom flask was added dimethyl 2,3,5,6,8,9-hexahydrothienol[3,4-b][1,4,7,10]tetraoxacyclododecine-11,13, dicarboxylic acid (0.460 mg, 1.44 mmols, 1 eq.) and copper chromite (110 mg, 0.346 mmols, 0.24 eq.). The vessel was evacuated from air and recharged with argon (this cycle process was done 3 times before backfilling with argon). Afterwards, 10 mL of quinoline was added and the reaction was wrapped with aluminum foil and left to stir at 150°C for a full day. Afterwards, the reaction was left to cool at room temperature and then poured into a 1 M HCl solution. The product was extracted out of the 1M HCl solution with diethyl ether, washed with distilled water, and then brine. The diethyl ether fraction was collected, dried over with sodium sulfate, filtered, and concentrated under vacuum. The crude product was purified by column chromatography using 100% EtOAc to afford a yellow liquid (90% yield).

13) 2,5-dibromo-2,3,5,6,8,9-hexahydrothienol[3,4-b][1,4,7,10]tetraoxacyclododecine:

In a round bottom flask charged with a stir bar was added N-bromosuccinimide (286 mg, 1.61 mmols, 2.1 eq.) The reaction vessel was purged with Argon for 15 minutes before 20 mL of anhydrous THF was added and sealed completely. The reaction was placed on an ice bath at 0°C for 1 hour before 2,3,5,6,8,9-hexahydrothienol[3,4-b][1,4,7,10]tetraoxacyclododecine (0.176 g, 0.765 mmols, 1 eq.) was slowly added the ice bath was removed and left to continue to stir at room temperature overnight in the dark. Afterwards, the reaction was concentrated in vacuo, redissolved in diethyl ether, and washed with water (x3) and brine (x1). The organic layers were collected, dried

over with sodium sulfate, filtered, and concentrated in vacuo. The crude product was purified by precipitating in distilled water to receive a gray powder where purity was very good.

Polymer Synthesis: KCTP is an essential step during the catalytic polymerization cycle, enabling more control over the chain growth mechanism compared to other polymerization techniques, such as Suzuki and Stille couplings, that also require longer time (2-3 days) and high temperature ($>100^{\circ}\text{C}$), providing more reproducible materials.



Scheme S4. Synthesis of polymers using KCTP/GRIMS polymerization

Poly(3-hexylthiophene-2,5-diyl) (P3HT): In a 3-neck round bottom flask charged with a stir bar was added 2,5-dibromo-3-hexylthiophene (0.500 g, 1.53 mmols, 1 eq.) dissolved in 10 mL of anhydrous THF. The reaction vessel was sealed and purged with argon for 30 minutes. The reaction vessel was placed on an ice bath and a mixture of isopropyl magnesium chloride (770 μL , 1.53 mmols, 1 eq.), LiCl (65 mg, 1.53 mmols, 1 eq.) and additional anhydrous THF (5 mL) was slowly added by dropwise addition to the stirring mixture. After 30 minutes of stirring at 0°C , the reaction was placed on an oil bath at 60°C and stirred for 2 hours before dichloro[1,3-bis(diphenylphosphino)propane]nickel (25 mg, 0.045 mmols, 0.05 eq.) was added, and the

reaction was left to stir overnight at 60°C. The reaction was then removed from the hot plate, cooled to room temperature, and then slowly added to 500 mL of distilled water stirring vigorously. After 10 minutes a black precipitate immediately forms, filtered, and dried at 60°C under vacuum overnight. The solid powder was subjected to Soxhlet purification with methanol, acetone, hexanes, and chloroform. The chloroform fraction was collected and concentrated in vacuo to receive a dark black powder.

Poly(tert-butyldimethyl(thiophene-3-ylmethoxysilane-2,5-diyl) (PT-OTBS): In a 3-neck round bottom flask charged with a stir bar was added tert-butyl(2,5-dibromothiophen-3-6)methoxy)dimethylsilane (0.500 g, 1.30 mmols, 1 eq.) dissolved in 10 mL of anhydrous THF. The reaction vessel was sealed and purged with argon for 30 minutes. The reaction vessel was placed on an ice bath and a mixture of isopropyl magnesium chloride (650 µL, 1.30 mmols, 1 eq.), LiCl (55 mg, 1.30 mmols, 1 eq.) and additional anhydrous THF (5 mL) was slowly added by dropwise addition to the stirring mixture. After 30 minutes of stirring at 0°C, the reaction was placed on an oil bath at 60°C and stirred for 2 hours before dichloro[1,3-bis(diphenylphosphino)propane]nickel (21 mg, 0.04 mmoles, 0.05 eq.) was added, and the reaction was left to stir overnight at 60°C. The reaction was then removed from the hot plate, cooled to room temperature, and then slowly added to 500 mL of 5M HCl solution stirring vigorously. After 10 minutes a black precipitate immediately forms, filtered, and dried at 60°C under vacuum overnight. The solid powder was subjected to Soxhlet purification with methanol followed by chloroform. The chloroform was collected and concentrated in vacuo to receive a dark black powder.

Poly(3-thiophenemethanol-2,5-diyl) (PTOH): In a round bottom flask charged with a stir bar was added poly(tert-butyl(dimethyl)thiophene-3-methoxy)silane (PT-OTBS) (200 mg) and the reaction vessel was sparged with argon continuously for 30 minutes before sealing the vessel. The polymer was dissolved in 15 mL of anhydrous THF before adding 4 mL of 1.0 M TBAF solution. The reaction vessel immediately turned to a dark red solution. The vessel was then placed on an oil bath at 60°C and left to stir overnight. The solution was then concentrated in vacuo, the gummy precipitate was suspending in diethyl ether and filtered. The filtrate was further washed with distilled water continuously. The collected powder was then dried in a vacuum oven at 60°C overnight. Afterwards, the powder was subjected to Soxhlet purification with pure methanol and diethyl ether. The powder was then placed under vacuum at 60°C overnight to receive a pure fine black powder.

Representative copolymer Synthesis: P3HT-co-PTOH:

In a 3-neck round bottom flask charged with a stir bar was added 2,5-dibromo-3-hexylthiophene (0.400 g, 1.23 mmols, 1 eq.) and tert-butyl(2,5-dibromothiophen-3-yl)methoxydimethylsilane (71 mg, 0.184 mmols, 0.15 eq.) dissolved in 10 mL of anhydrous THF. The reaction vessel was sealed and purged with argon for 30 minutes. The reaction vessel was placed on an ice bath and a mixture of isopropyl magnesium chloride (705 μ L, 1.44 mmols, 1.15 eq.), LiCl (60 mg, 1.44 mmols, 1.15 eq.) and an additional anhydrous THF (5 mL) was slowly added by dropwise addition to the stirring mixture. After 30 minutes of stirring at 0°C, the reaction was placed on an oil bath at 60°C and stirred for 2 hours before dichloro[1,3-bis(diphenylphosphino)propane]nickel

(38 mg, 0.071 mmols, 0.05 eq.) was added, and the reaction was left to stir overnight at 60°C. The reaction was then removed from the hot plate, cooled to room temperature, and then slowly added to 500 mL of distilled water stirring vigorously. After 10 minutes a black precipitate immediately forms, filtered, and dried at 60°C under vacuum overnight. The solid powder was subjected to Soxhlet purification with methanol, acetone, hexanes, and chloroform. The chloroform fraction was collected and concentrated in vacuo to receive a dark black powder. It was reported that the ratio of less hindered to more hindered thiophene-Grignard formation is 85:15, but the regioregularity is higher than that, so the mechanism is not straightforward. The GRIM polymerization mechanism involves multiple intermediates, catalyst structures, and steric/coordination effects from substituents. In particular, the crown thiophenes are symmetric and 3-4-disubstituted, and the O-t-butyl dimethylsilyl monomer would be particularly sterically hindered, which may lead to deviations from the intended monomer incorporation ratios. See Loewe, R.S.; Ewbank, P.C.; Liu, J.; Zhai, L.; and McCullough, R.D., *Macromolecules* 2001, 34,13:4324-4333. Doi:10.1021/ma001677+.

NMR Spectra:

Monomer NMR Spectra:

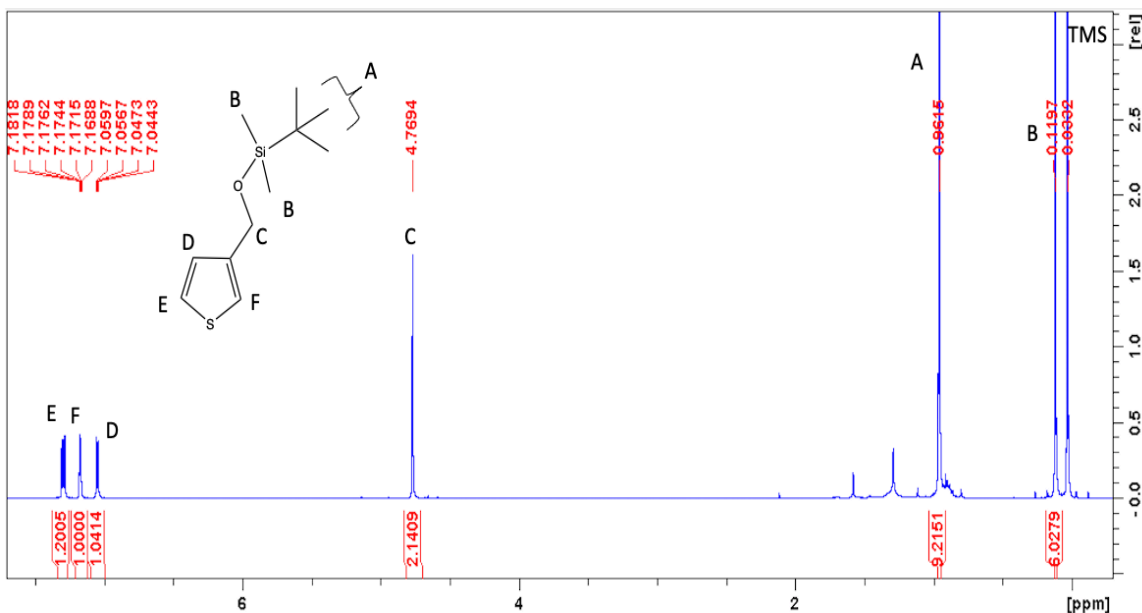


Figure S1. ¹H NMR (300 MHz, Chloroform-d) of Tert-butyldimethyl(thiophen-3-ylmethoxy)silane: δ 0.12 (t, 6H), 0.96 (t, 3H), 4.77 (t, 2H), 7.0-7.1 (d, 1H), 7.17 (s, 1H), 7.1 (d, 1H), and 7.17-7.18 (d, 1H).

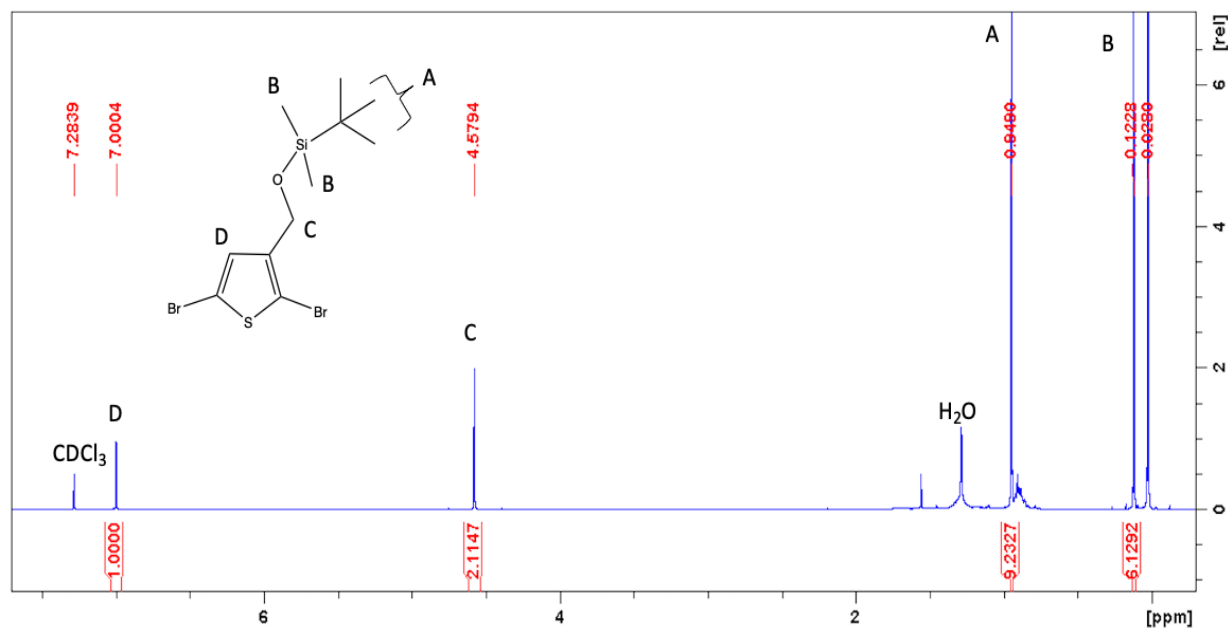


Figure S2. ¹H NMR (300 MHz, Chloroform-d) of Tert-butyl(2,5-dibromothiophen-3-ylmethoxy)dimethylsilane: δ 0.12 (t, 6H), 0.95 (t, 3H), 4.58 (t, 2H), and 7.0 (s, 1H).

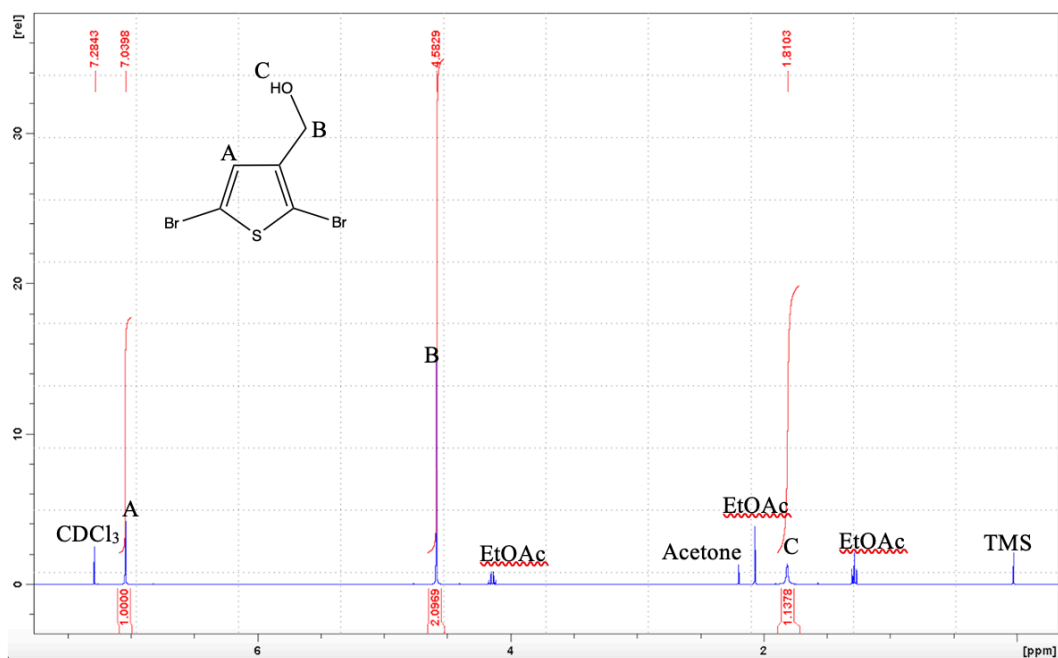


Figure S3. ¹H NMR (300 MHz, Chloroform-d) of (2,5-dibromothiophen-yl)methanol: δ 1.81 (s, 1H), 4.58 (t, 2H), and 7.04 (s, 1H).

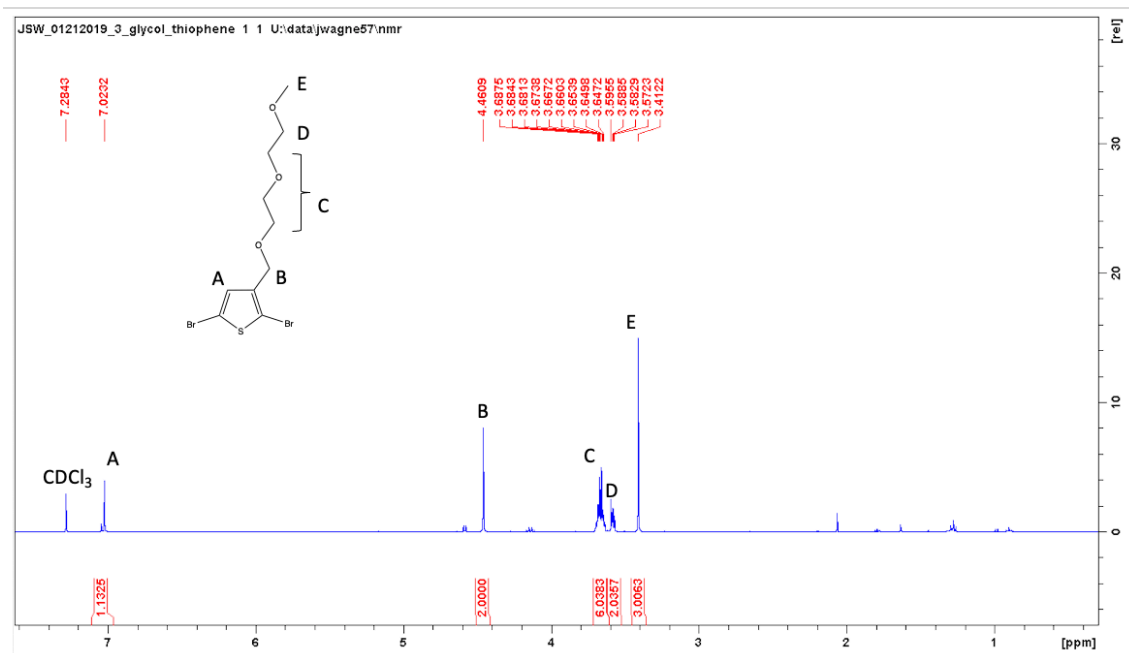


Figure S4. ¹H NMR (300 MHz, Chloroform-d) of 2,5-dibromo-3-((2-(2-methoxyethoxy)ethoxy)methyl)thiophene: δ 3.41 (t, 3H), 3.57-3.59 (m, 2H), 3.64-3.69 (m, 6H), 4.46 (t, 2H), and 7.03 (s, 1H).

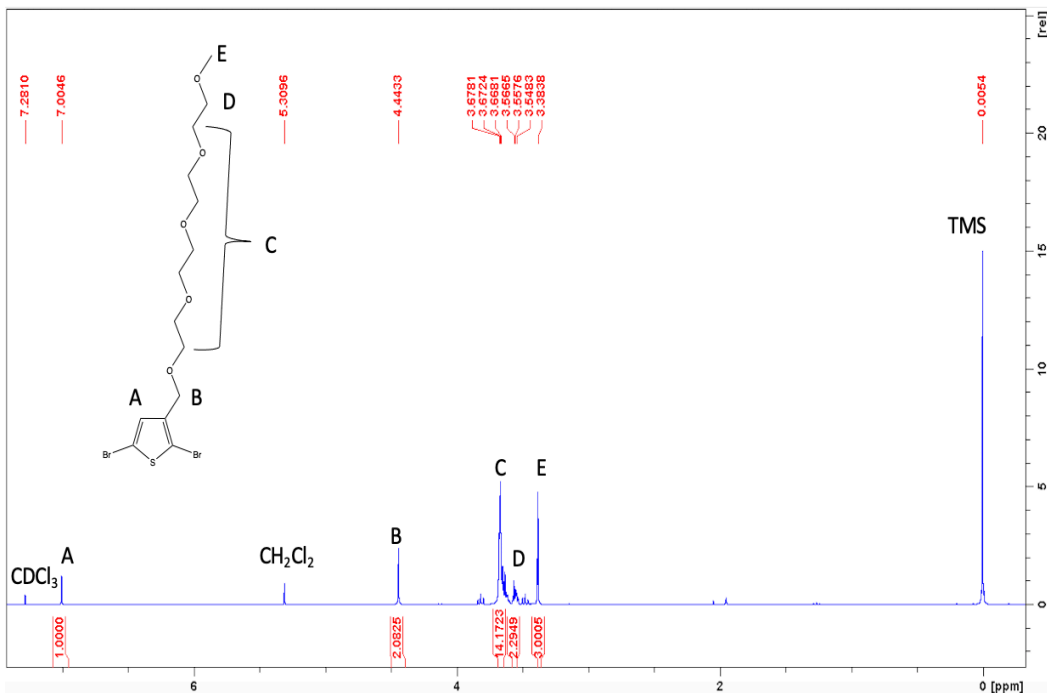


Figure S5. ¹H NMR (300 MHz, Chloroform-d) of 2,5-dibromo-3-(2-(2-(2-(2-methoxyethoxy)ethoxy)ethoxy)ethyl)thiophene: δ 3.38 (t, 3H), 3.55-3.57 (m, 2H), 3.67-3.68 (m, 14H), 4.44 (t, 2H), and 7.00 (s, 1H).

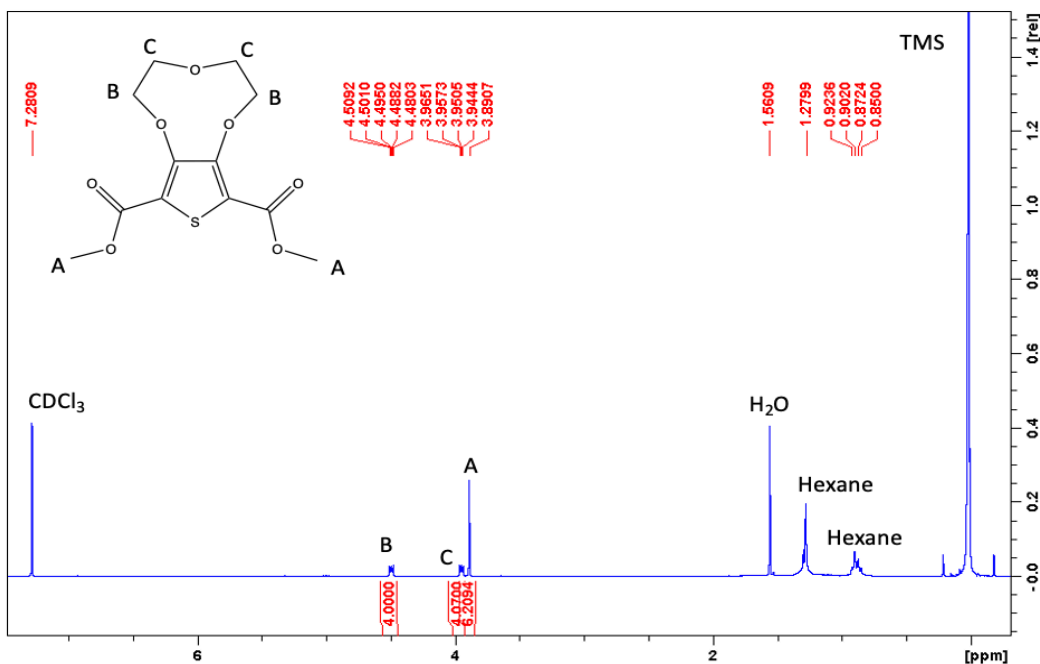


Figure S6. ¹H NMR (300 MHz, Chloroform-d) of Dimethyl 2,3,5,6-tetrahydrothieno[3,4-b][1,4,7]trioxonine-8.10-dicarboxylate [3-crown-dicarboxylate-thiophene: δ 3.89 (t, 6H), 3.94-3.97 (d, 4H), and 4.48-4.51 (d, 4H).

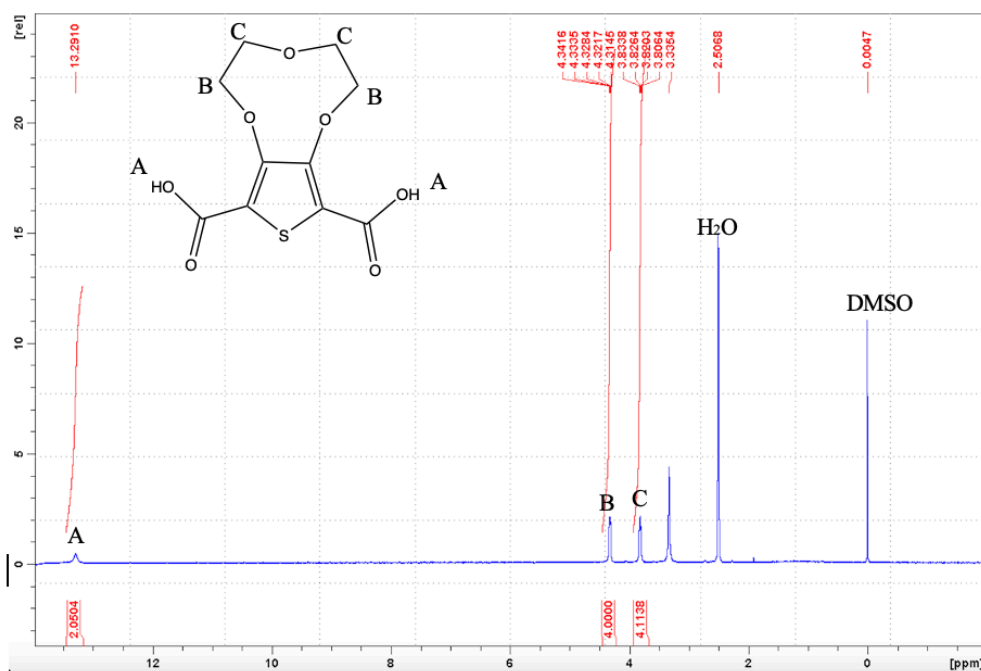


Figure S7. ^1H NMR (300 MHz, DMSO- d_6) of Dimethyl 2,3,5,6-tetrahydrothieno[3,4-b][1,4,7]trioxonine-8,10-dicarboxylic acid [3-crown-dicarboxylic acid-thiophene: δ 3.81-3.83 (d, 4H), 4.31-4.34 (d, 4H), and 13.29 (s, 2H).

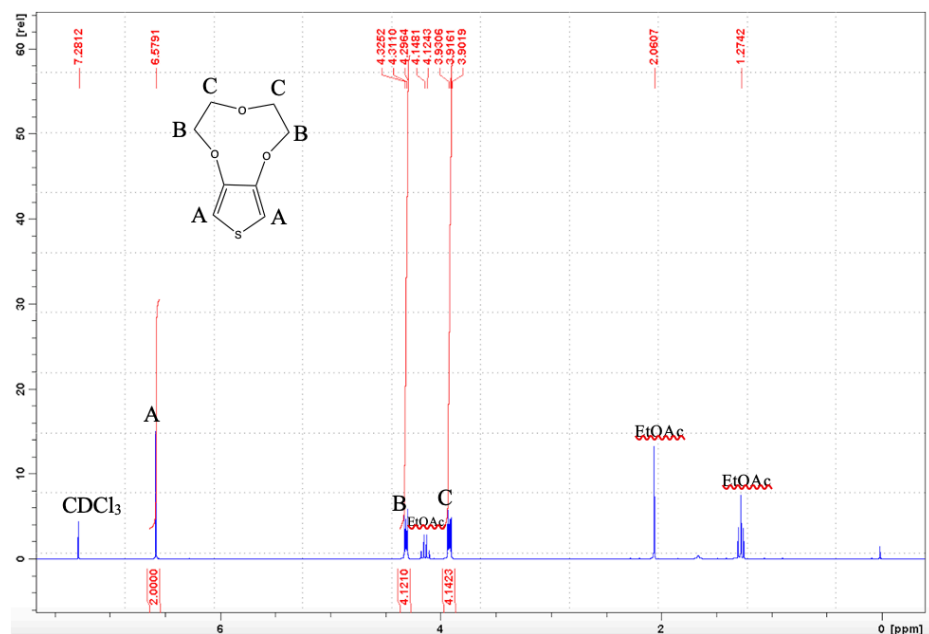


Figure S8. ^1H NMR (300 MHz, Chloroform- d) of 2,3,5,6-tetrahydrothieno[3,4-b][1,4,7]trioxonine [3-crown thiophene: δ 3.90-9.93 (m, 4H), 4.30-4.33 (m, 4H), and 6.58 (s, 2H).

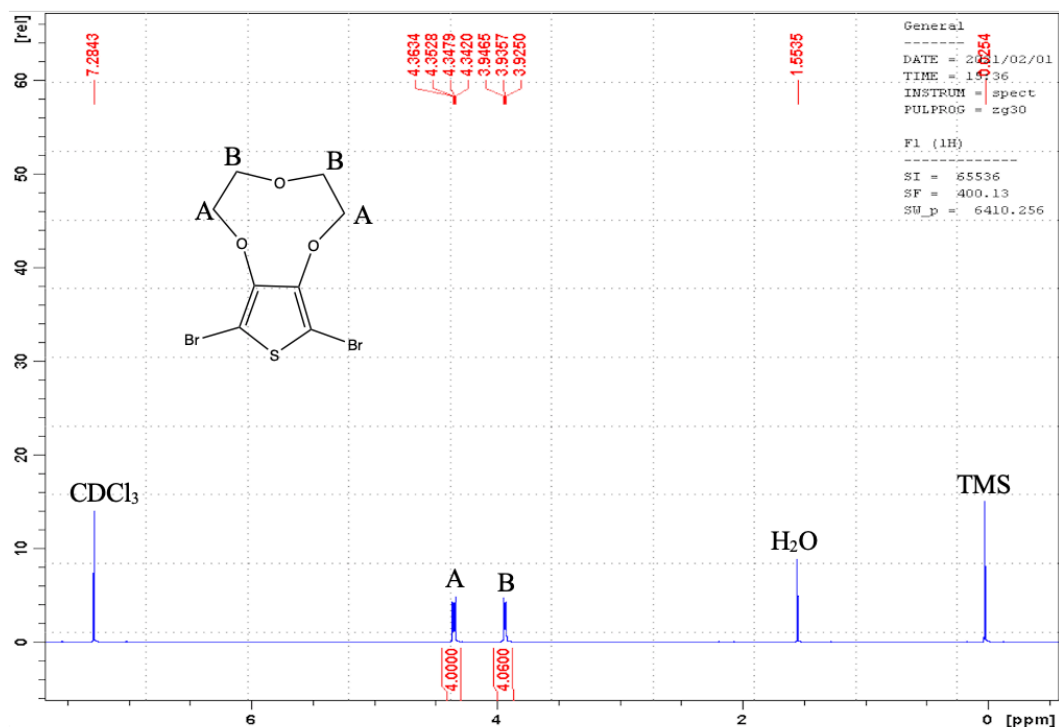


Figure S9. ¹H NMR (300 MHz, Chloroform-d) of 2,5-dibromo-2,3,5,6-tetrahydroethieno[3,4-b][1,4,7]trioxone: δ 3.93-3.95 (d, 4H), 4.34-4.36 (d, 4H).

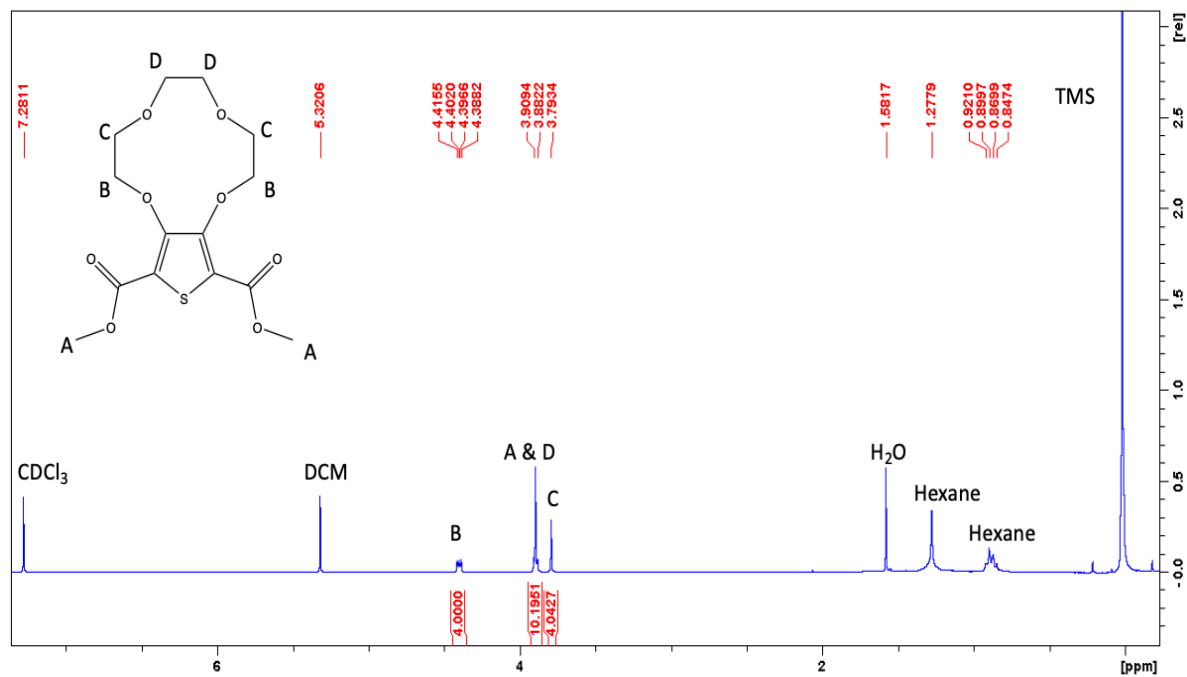


Figure S10. ¹H NMR (300 MHz, Chloroform-d) of Dimethyl 2,3,5,6,8,9-hexahydrothienol[3,4-b][1,4,7,10]tetraoxacyclododecine-11,13, dicarboxylate [4-crown-dicarboxylate-thiophene]: δ 3.79 (t, 4H), 3.88-3.90 (m, 10H), and 4.39-4.41 (d, 4H).

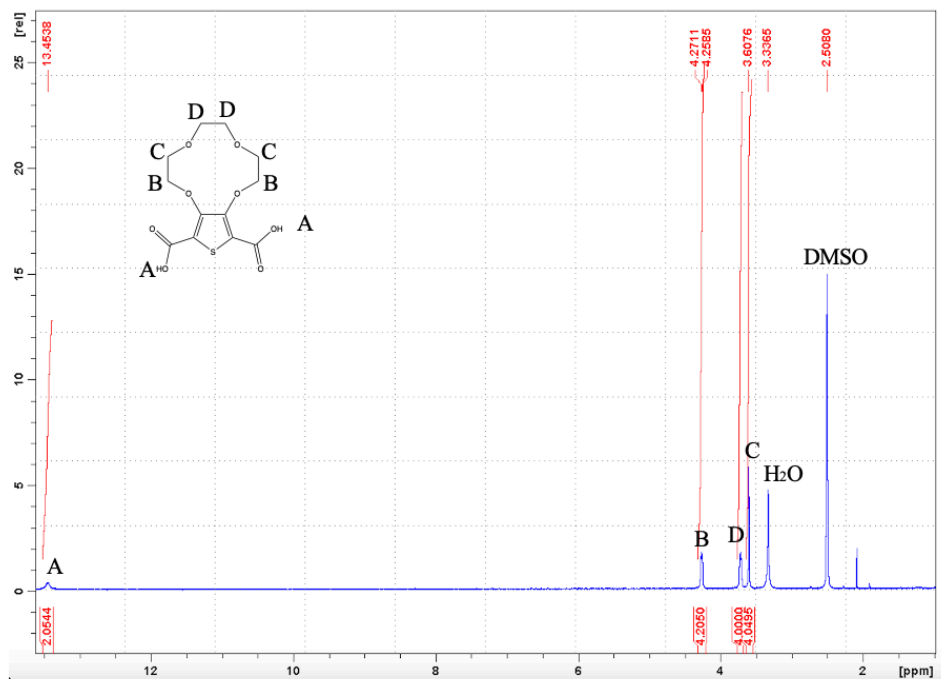


Figure S11. ^1H NMR (300 MHz, DMSO-d_6) of Dimethyl 2,3,5,6,8,9-hexahydrothienol[3,4-b][1,4,7,10]tetraoxacyclododecine-11,13, dicarboxylic acid [4-crown-dicarboxylic acid-thiophene]: δ 3.61 (t, 4H), 3.7-3.8 (m, 4H), 4.26-4.27 (m, 4H), and 13.45 (s, 2H).

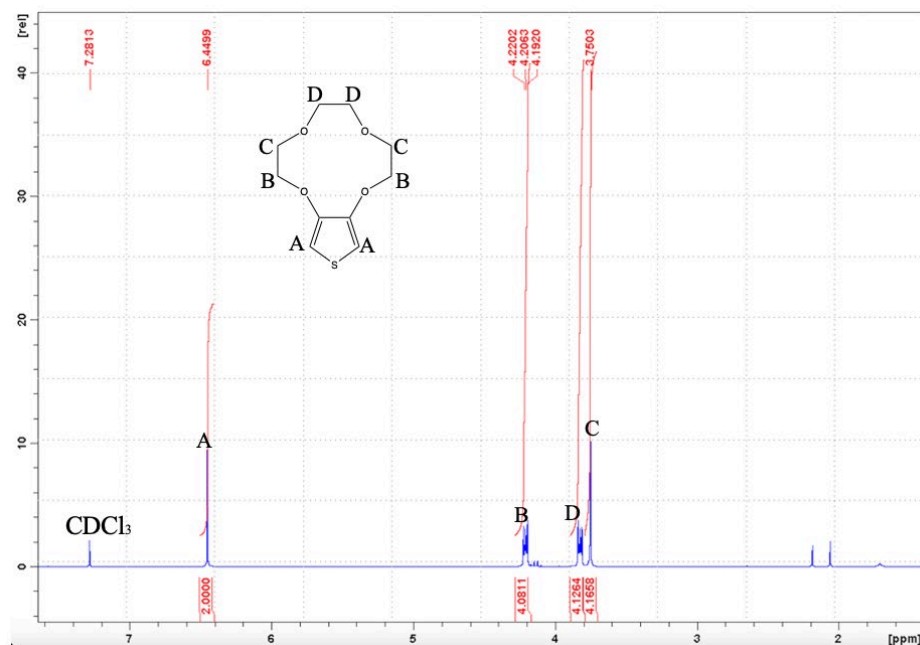


Figure S12. ^1H NMR (300 MHz, Chloroform-d) of 2,3,5,6,8,9-hexahydrothienol[3,4-b][1,4,7,10]tetraoxacyclododecine [4-crown thiophene]: δ 3.75 (t, 4H), 3.80-3.85 (m, 4H), 4.19-4.22 (m, 4H), and 6.44 (s, 1H).

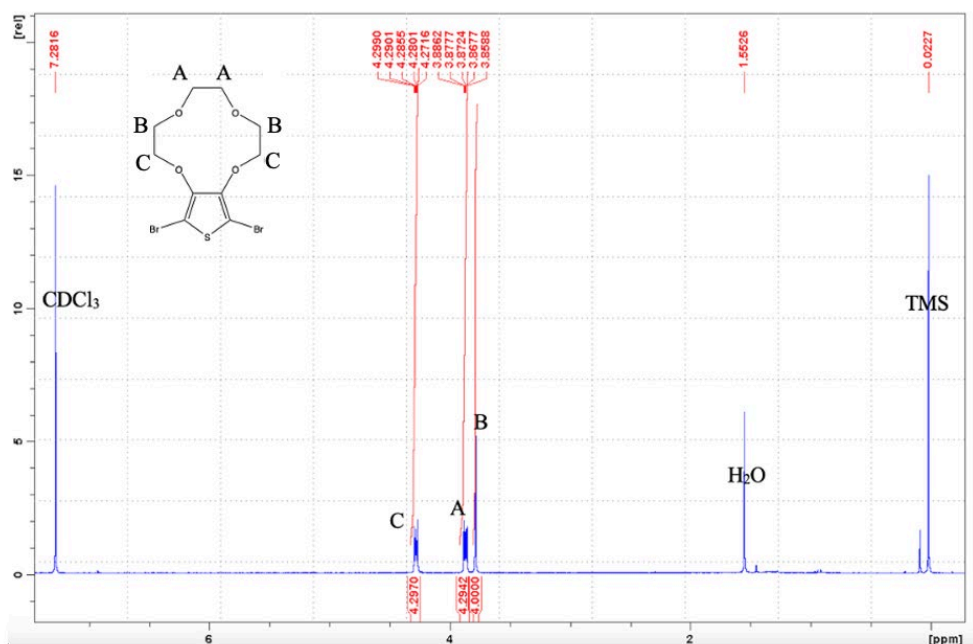


Figure S13. ^1H NMR (300 MHz, Chloroform-d) of 2,5-dibromo-2,3,5,6,8,9-hexahydrothienol[3,4-b][1,4,7,10]tetraoxacyclododecine: δ 3.86 (t, 4H), 3.86-3.89 (m, 4H), and 4.27-4.29 (m, 4H).

Polymer NMR Spectra:

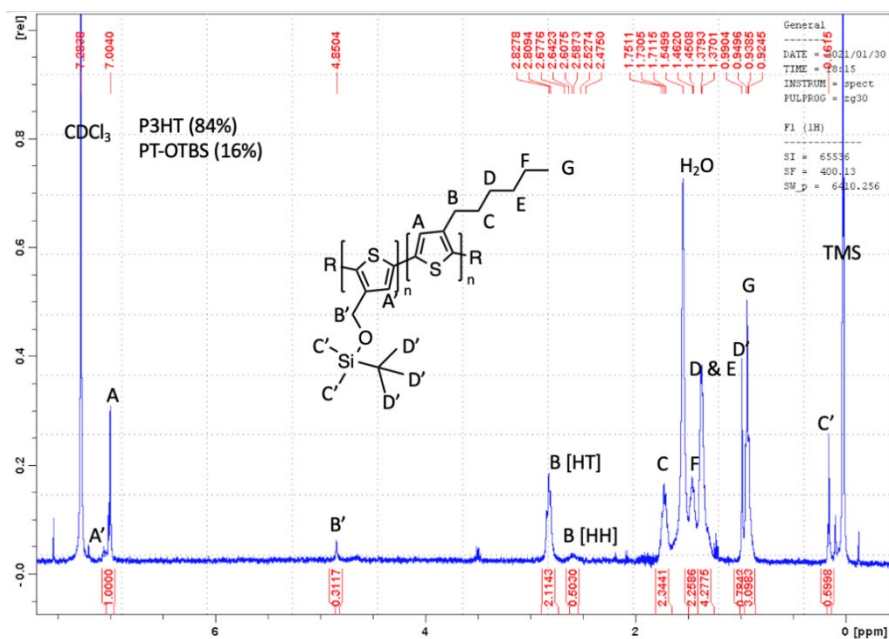


Figure S14. ^1H NMR (300 MHz, Chloroform-d) of P3HT-co-PTOTBS: δ 0.162 (t, 6H), 0.92-0.94 (t, 3H), 0.99 (9H), 1.37-1.38 (m, 4H), 1.45-1.46 (m, 2H), 1.71-1.75 (m, 2H), 2.59-2.83 (t, 2H), 4.85 (t, 2H), 7.00 (s, 1H), 7.1 (s, 1H).

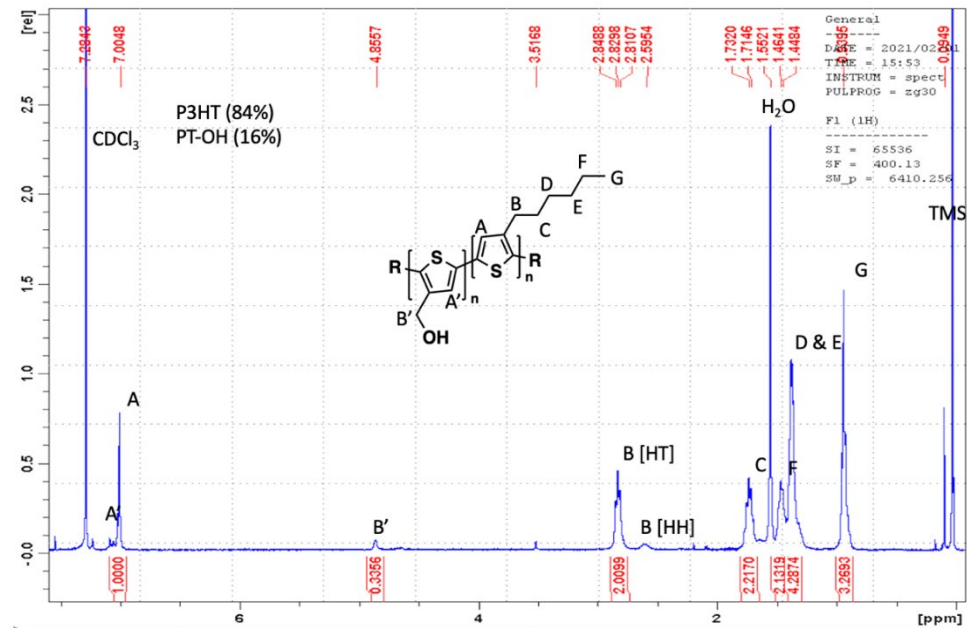


Figure S15. ^1H NMR (300 MHz, Chloroform- d) of P3HT-co-PTOH: δ 0.94 (t, 3H), 1.45-1.46 (m, 4H), 1.71-1.73 (m, 2H), 2.81-2.85 (t, 2H), 4.86 (t, 1H), 7.00 (s, 1H), 7.1 (s, 1H).

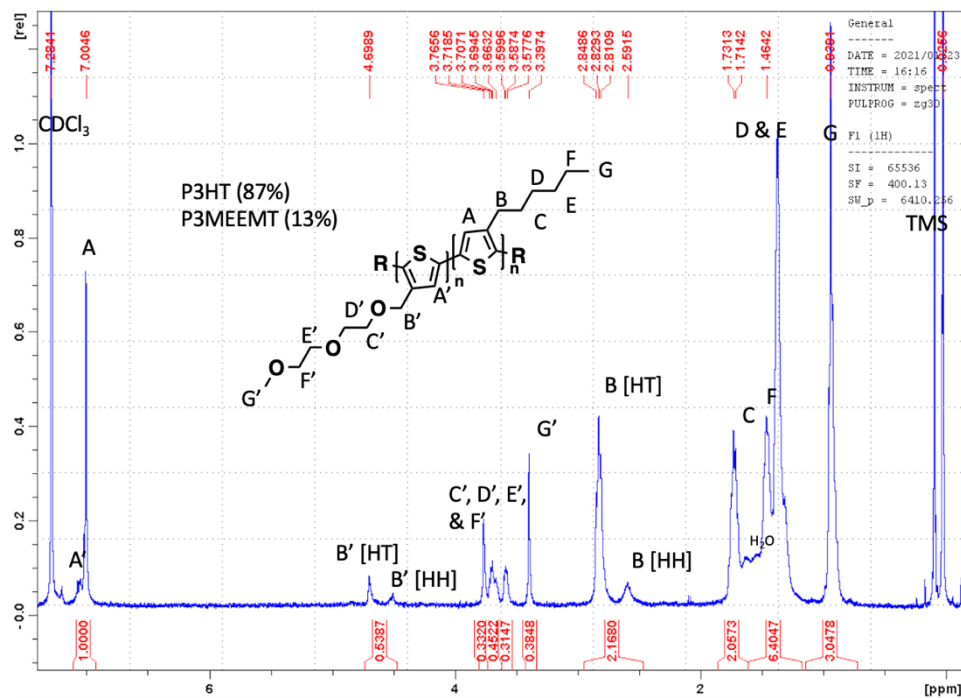


Figure S16. ^1H NMR (300 MHz, Chloroform- d) of P3HT-co-P3MEEMT: δ 0.94 (t, 3H), 1.45-1.46 (m, 4H), 1.71-1.73 (m, 2H), 2.81-2.85 (t, 2H), 3.40 (t, 3H), 3.58-3.77 (m, 8H), 4.70 (t, 2H), 7.00 (s, 1H), 7.1 (s, 1H).

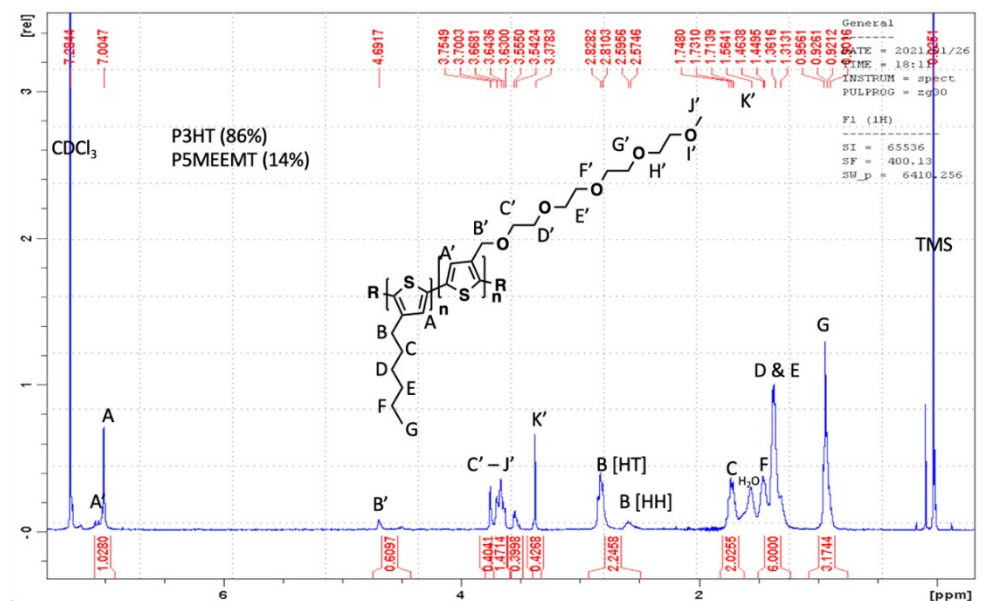


Figure S17. ¹H NMR (300 MHz, Chloroform-d) of P3HT-co-P5MEEMT: δ 0.90-0.96 (t, 3H), 1.31-1.46 (m, 4H), 1.71-1.75 (m, 2H), 2.81-2.83 (t, 2H), 3.38 (t, 3H), 3.54-3.75 (m, 16H), 4.69 (t, 2H), 7.00 (s, 1H), 7.1 (s, 1H).

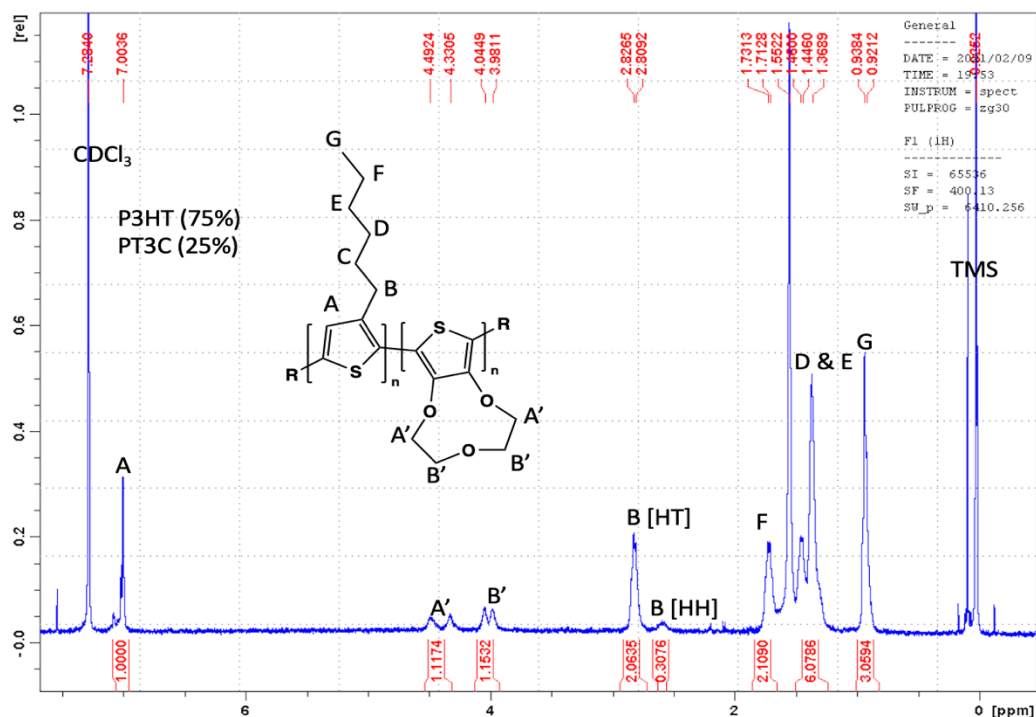


Figure S18. ¹H NMR (300 MHz, Chloroform-d) of P3HT-co-PT3C: δ 0.92-0.94 (t, 3H), 1.37-1.46 (m, 4H), 1.71-1.73 (m, 2H), 2.81-2.83 (t, 2H), 3.98-4.04 (d, 4H), 4.33-4.49 (d, 4H), 7.00 (s, 1H), 7.1 (s, 1H).

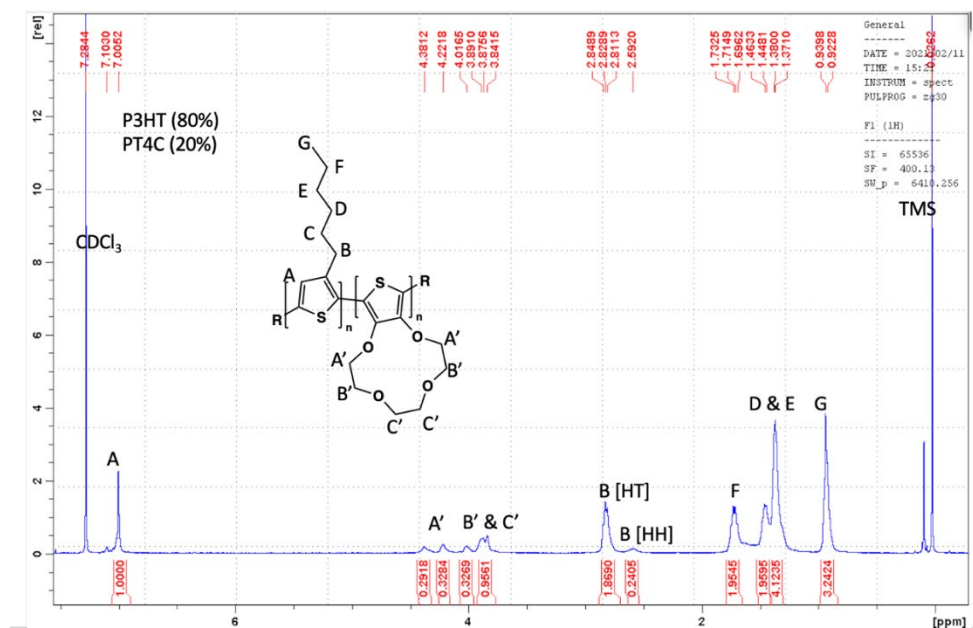


Figure S19. ¹H NMR (300 MHz, Chloroform-d) of P3HT-co-PT4C: δ 0.92-0.94 (t, 3H), 1.37-1.46 (m, 4H), 1.69-1.73 (m, 2H), 2.81-2.85 (t, 2H), 3.84-4.01 (m, 8H), 4.22-4.38 (d, 4H), 7.00 (s, 1H), 7.1 (s, 1H).

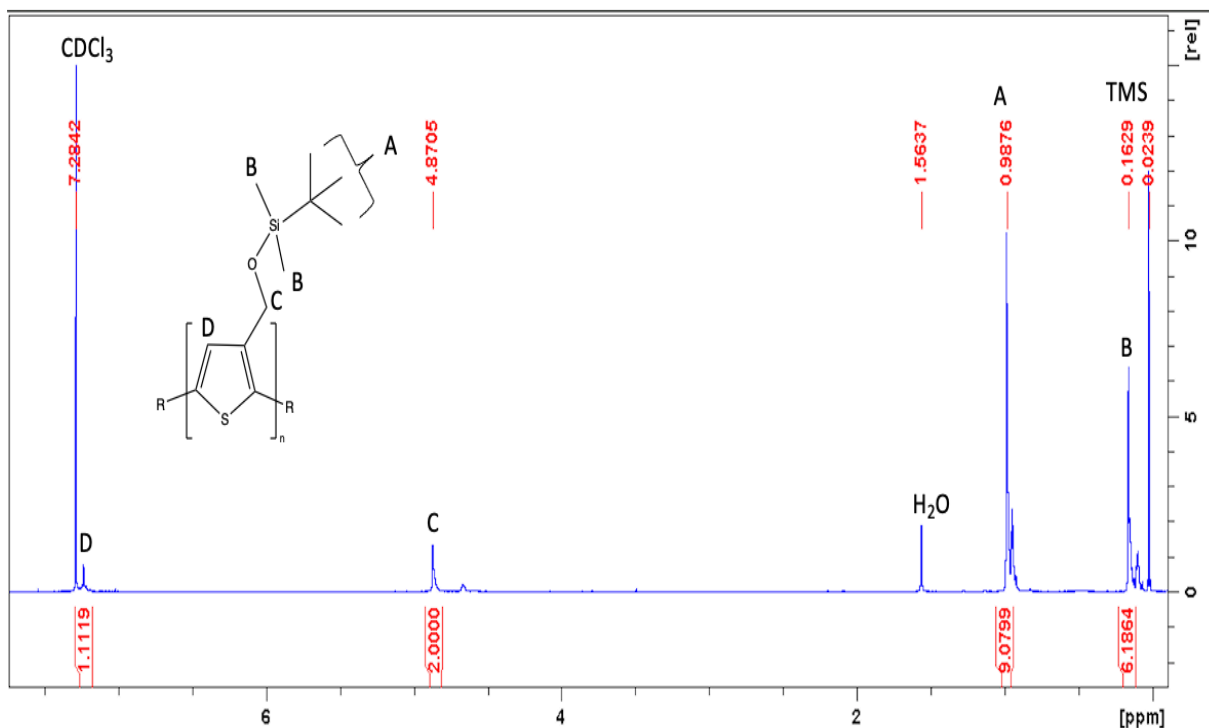


Figure S20. ¹H NMR (300 MHz, Chloroform-d) of PTOTBS: δ 0.162 (t, 6H), 0.99 (t, 9H), 4.87 (t, 2H), 7.28 (s, 1H).

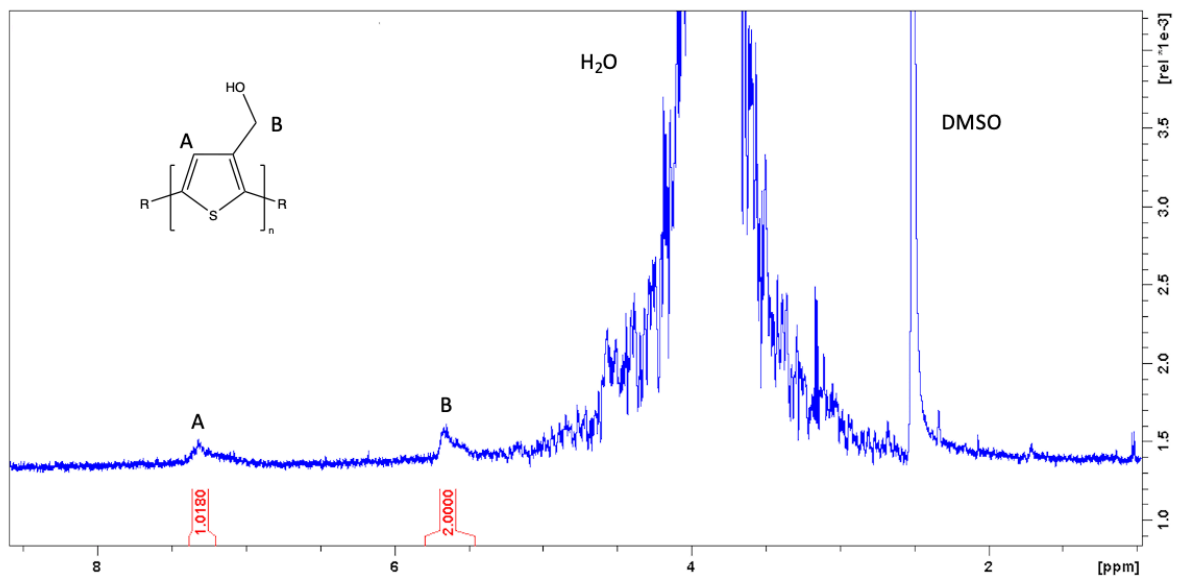


Figure S21. ^1H NMR (300 MHz, DMSO- d_6) of PTOH: δ 5.0-5.6 (m, 2H), 7.25 (s, 1H).

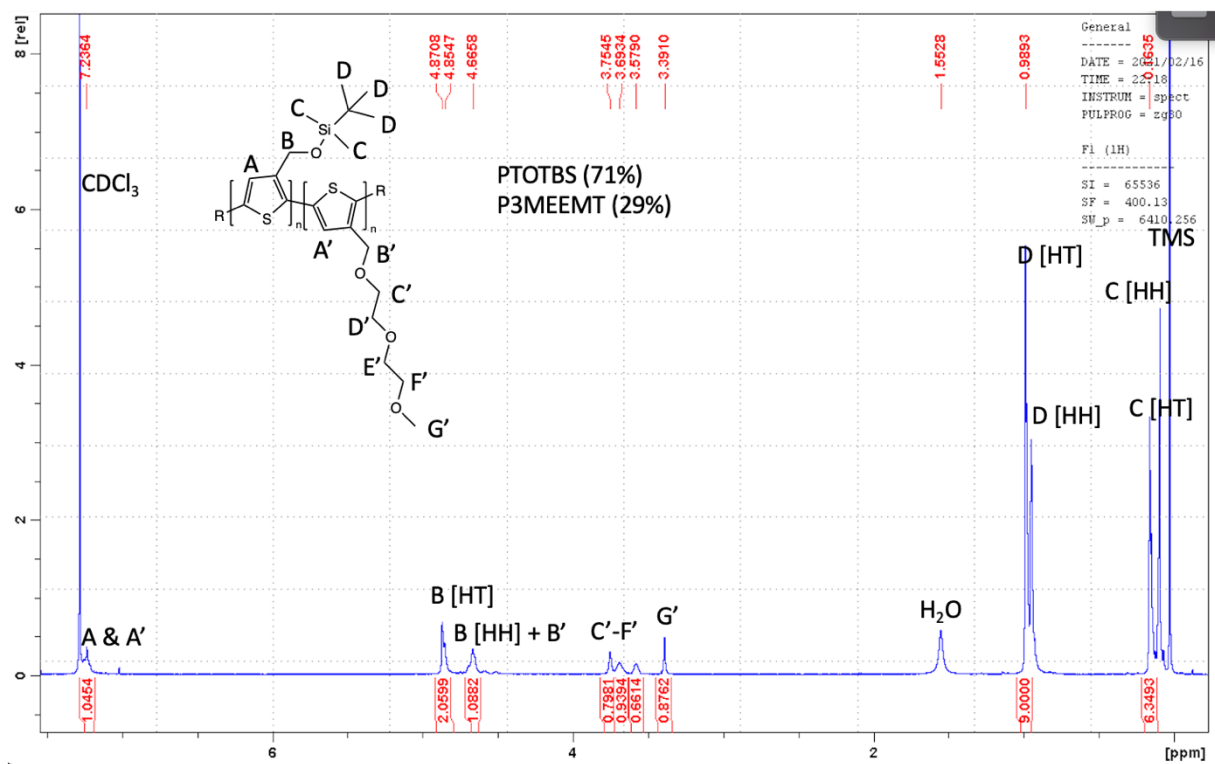


Figure S22. ^1H NMR (300 MHz, Chloroform- d) of PTOTBS-co-P3MEEMT: δ 0.164 (t, 6H), 0.99 (t, 9H), 3.39 (s, 3H), 3.58-3.75 (m, 8H), 4.67 (m, 2H), 4.85-4.87 (m, 2H), 7.24 (s, 1H), 7.25 (s, 1H).

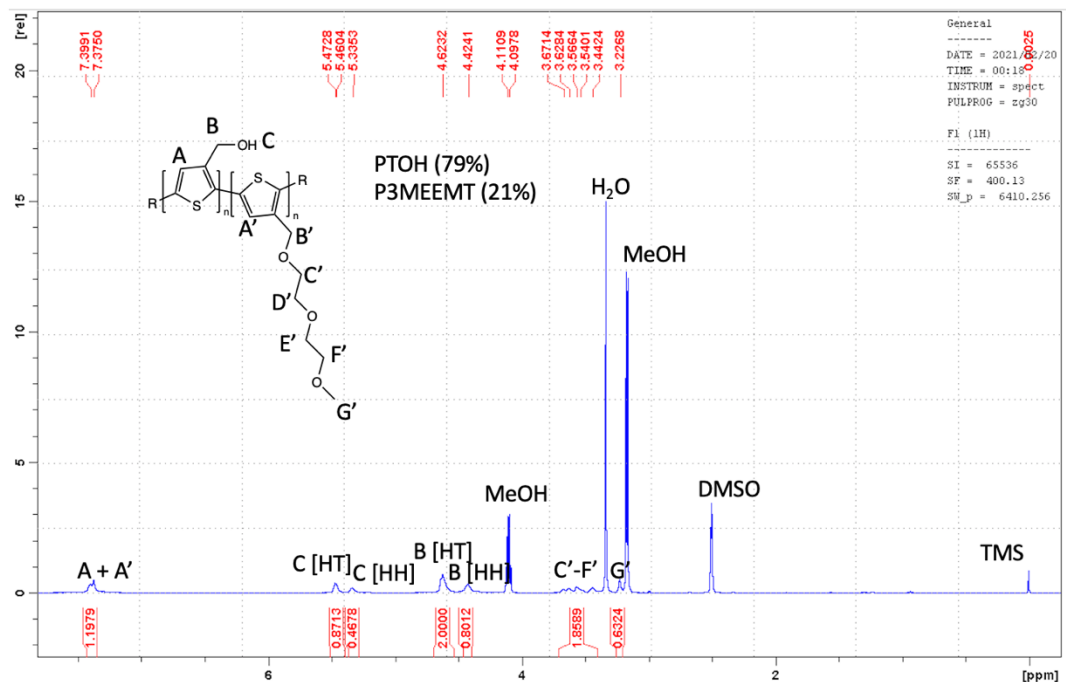


Figure S23. ¹H NMR (300 MHz, DMSO-d₆) of PTOH-co-P3MEEMT: δ 3.23 (t, 3H), 3.4-3.7 (m, 8H), 4.42 (t, 2H), 4.62 (t, 2H), 5.46-5.47 (s, 1H), 7.38-7.39 (m, 2H).

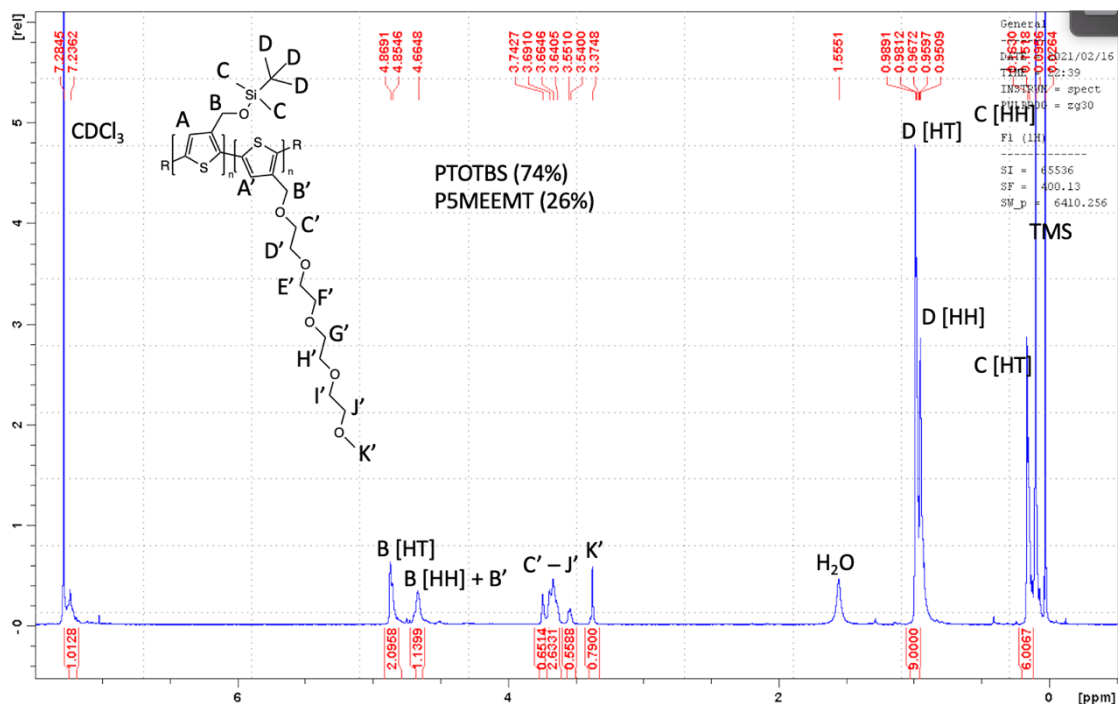


Figure S24. ¹H NMR (300 MHz, Chloroform-d) of PTOTBS-co-P5MEEMT: δ 0.163 (t, 6H), 0.95-0.99 (t, 9H), 3.37 (s, 3H), 3.54-3.74 (m, 16H), 4.66 (m, 2H), 4.85-4.87 (m, 2H), 7.24-7.28 (m, 2H).

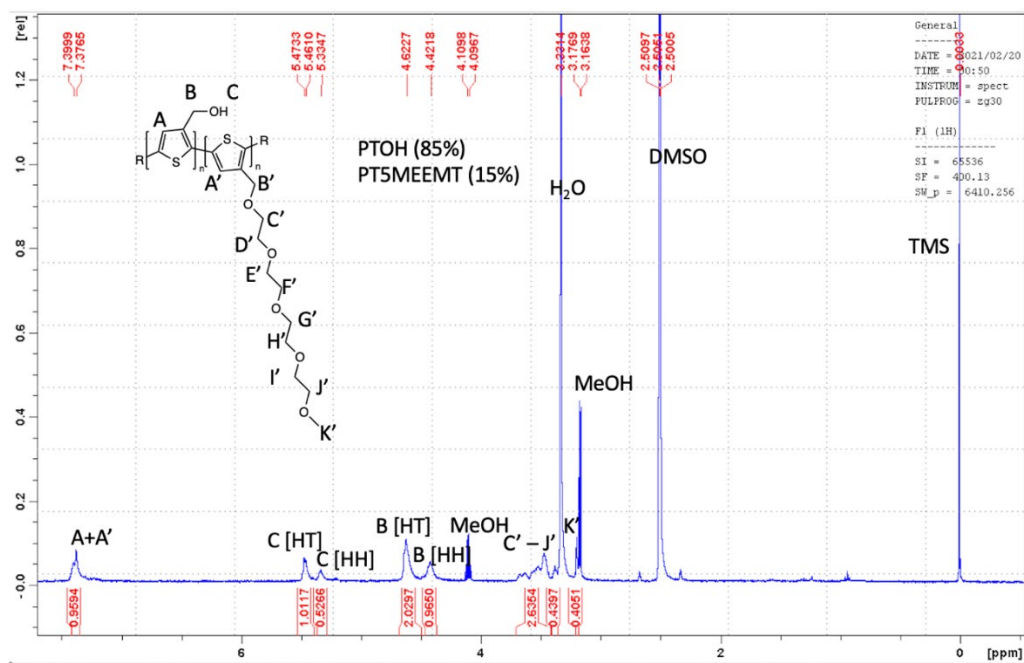


Figure S25. ¹H NMR (300 MHz, DMSO-d₆) of PTOH-co-P5MEEMT: δ 3.16-3.17 (t, 3H), 3.33-3.7 (m, 16H), 4.42 (t, 2H), 4.62 (t, 2H), 5.46-5.47 (s, 1H), 7.38-7.40 (m, 2H).

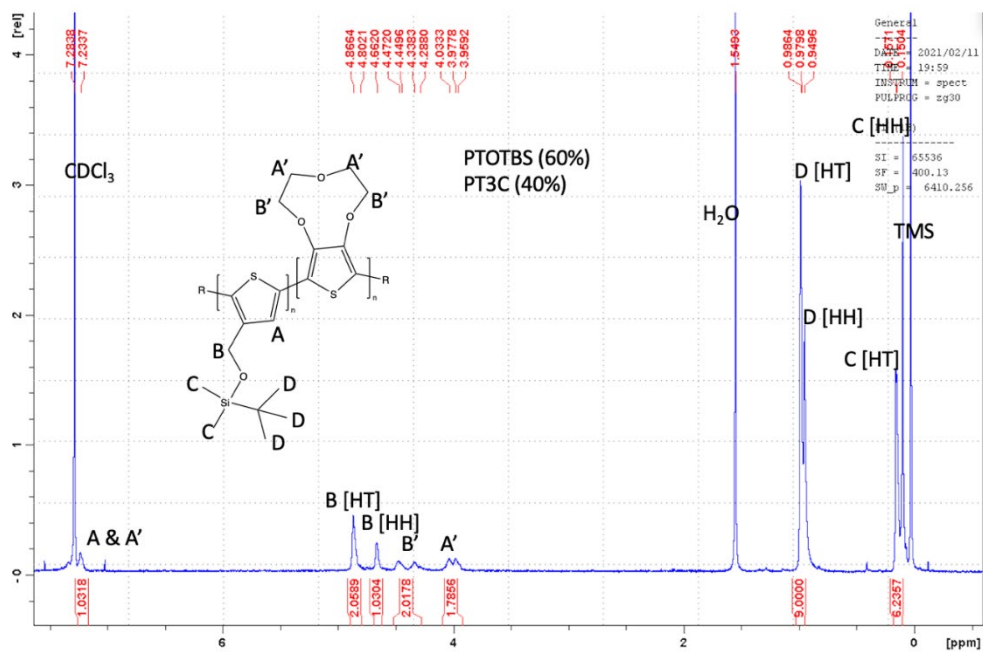


Figure S26. ¹H NMR (300 MHz, Chloroform-d) of PTOTBS-co-PT3C: δ 0.15 (t, 6H), 0.95-0.99 (t, 9H), 3.96-4.0 (m, 4H), 4.28-4.66 (m, 4H), 4.86 (t, 2H), 7.23-7.28 (m, 2H).

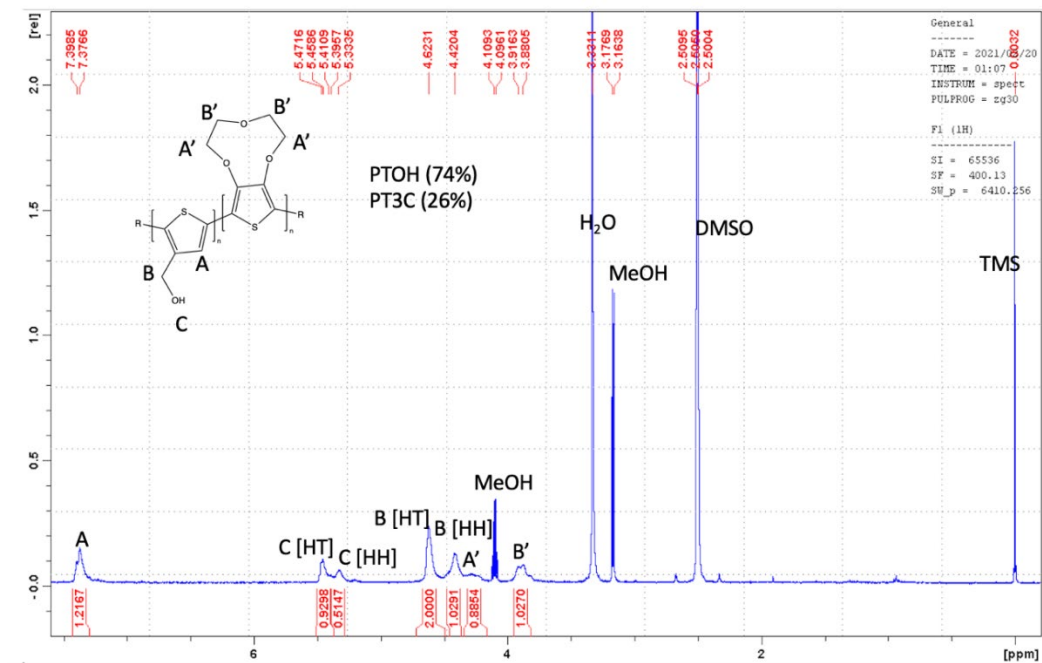


Figure S27. ¹H NMR (300 MHz, DMSO-d₆) of PTOH-co-PT3C: δ 3.88-3.92 (m, 4H), 4.1-4.11 (m, 4H), 4.62 (m, 2H), 5.3-5.48 (s, 1H), 7.38-7.40 (m, 2H).

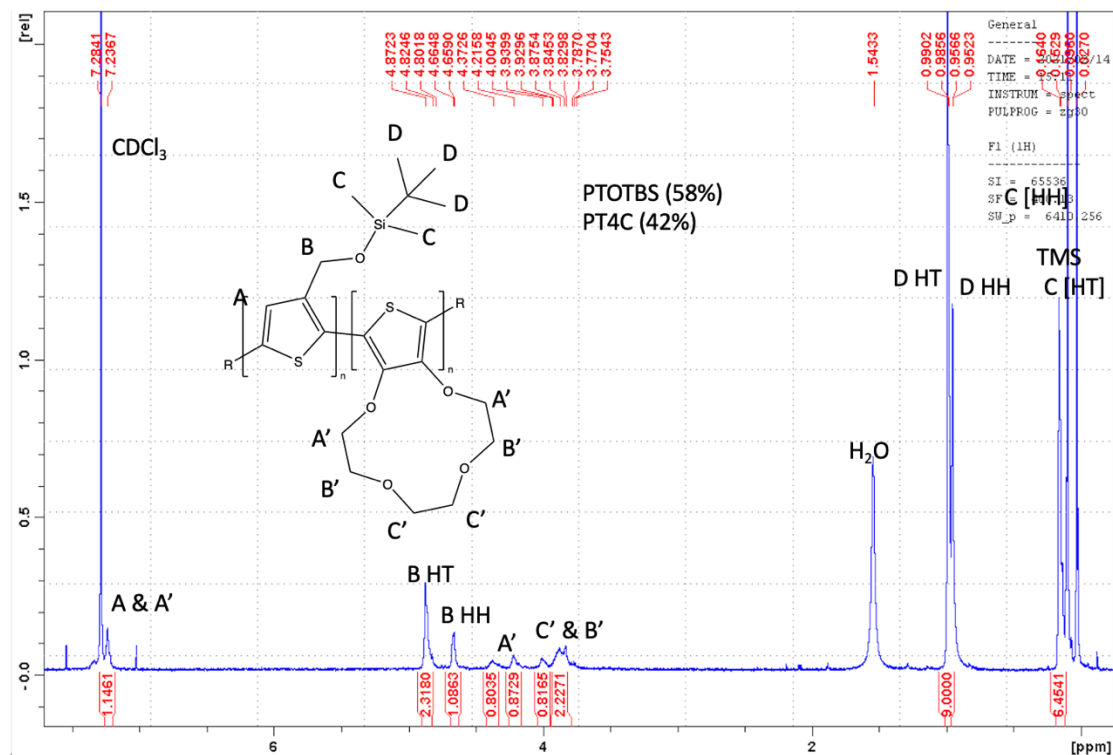


Figure S28. ¹H NMR (300 MHz, Chloroform-d) of PTOTBS-co-PT4C: δ 0.16 (t, 6H), 0.95-0.99 (t, 9H), 3.75-4.37 (m, 12H), 4.87 (t, 2H), 7.24-7.28 (m, 2H).

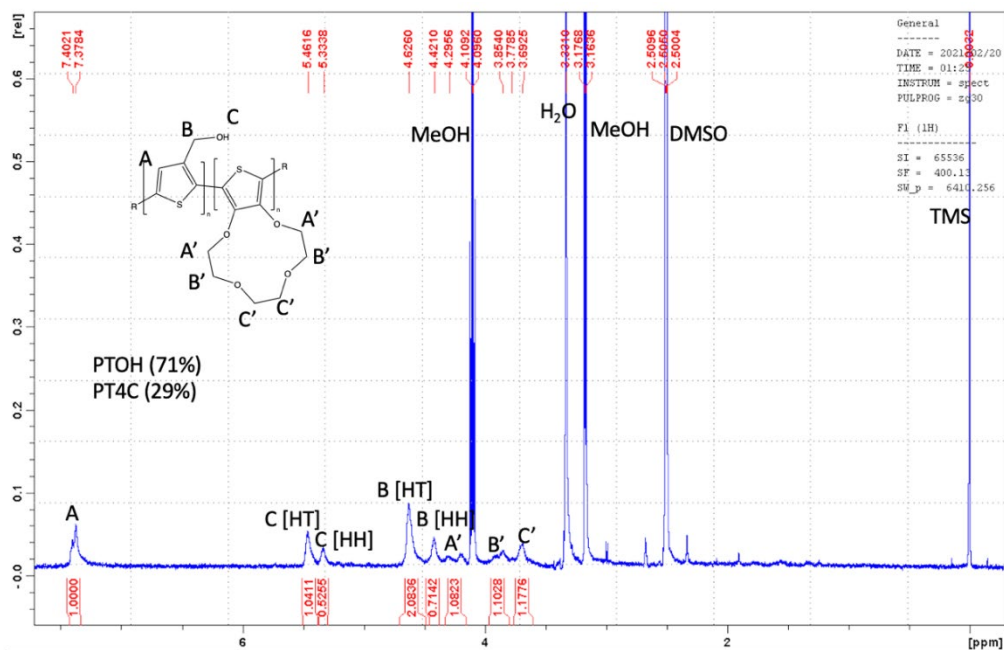


Figure S29. ¹H NMR (300 MHz, DMSO-d₆) of PTOH-co-PT4C: δ 3.69-3.38 (m, 8H), 4.1-4.3 (m, 4H), 4.62 (m, 2H), 5.46 (s, 1H), 7.37-7.40 (m, 2H).

Gel Permeation Chromatography (GPC)

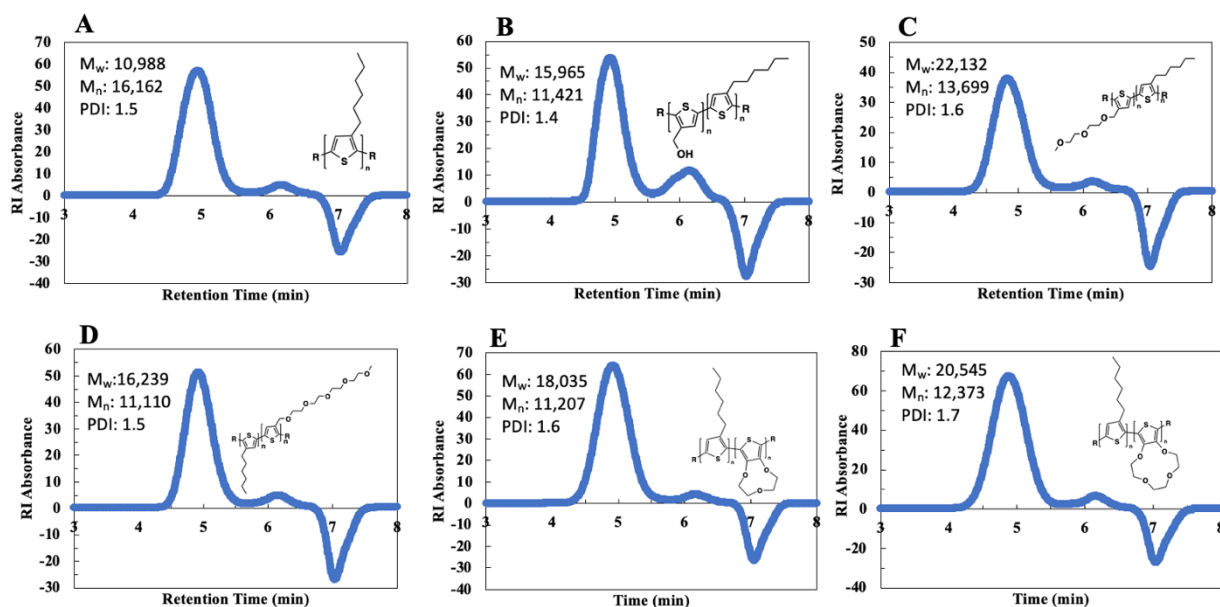


Figure S30. RI trace of A) P3HT, B) P3HT-co-PTOH, C) P3HT-co-P3MEEMT, D) P3HT-co-P5MEEMT, E) P3HT-co-PT3C, and F) P3HT-co-PT4C.

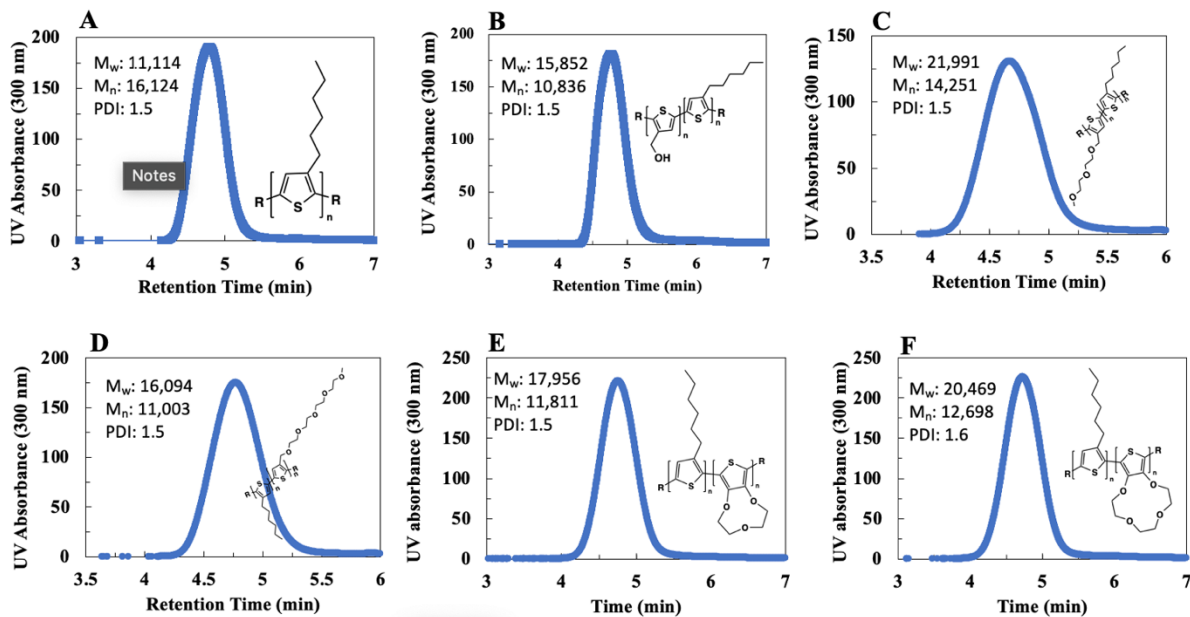


Figure S31. UV-SEC trace of A) P3HT, B) P3HT-co-PTOH, C) P3HT-co-P3MEEMT, D) P3HT-co-P5MEEMT, E) P3HT-co-PT3C, and F) P3HT-co-PT4C.

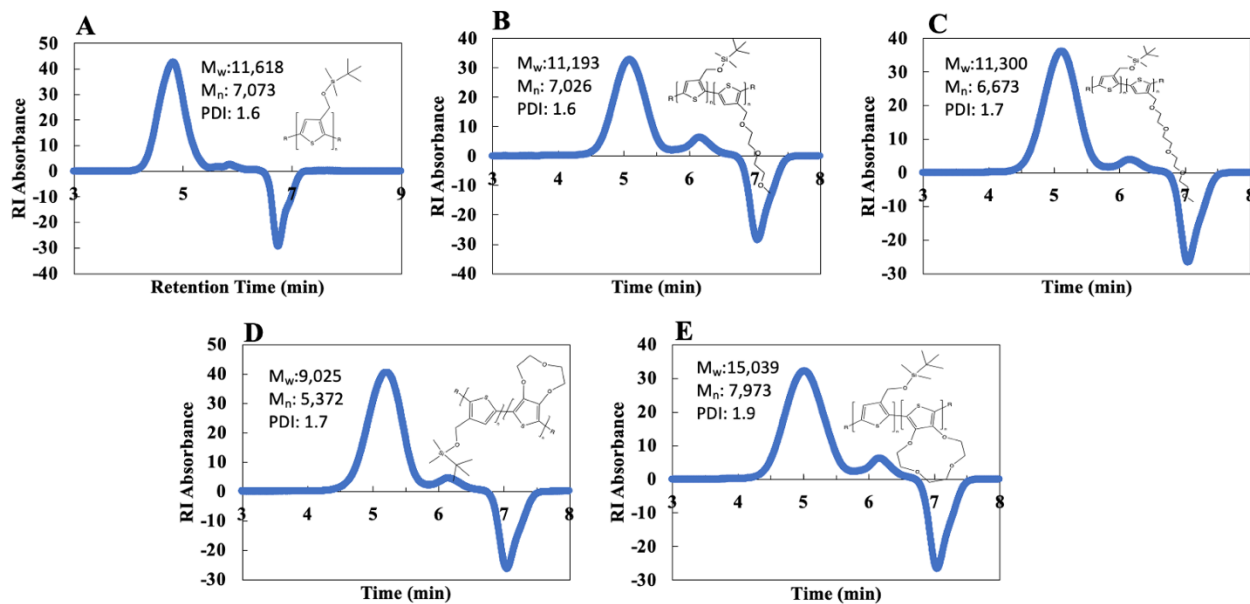


Figure S32. RI trace of A) PTOTBS, B) PTOTBS-co-P3MEEMT, C) PTOTBS-co-P5MEEMT, D) PTOTBS-co-PT3C, and E) PTOTBS-co-PT4C.

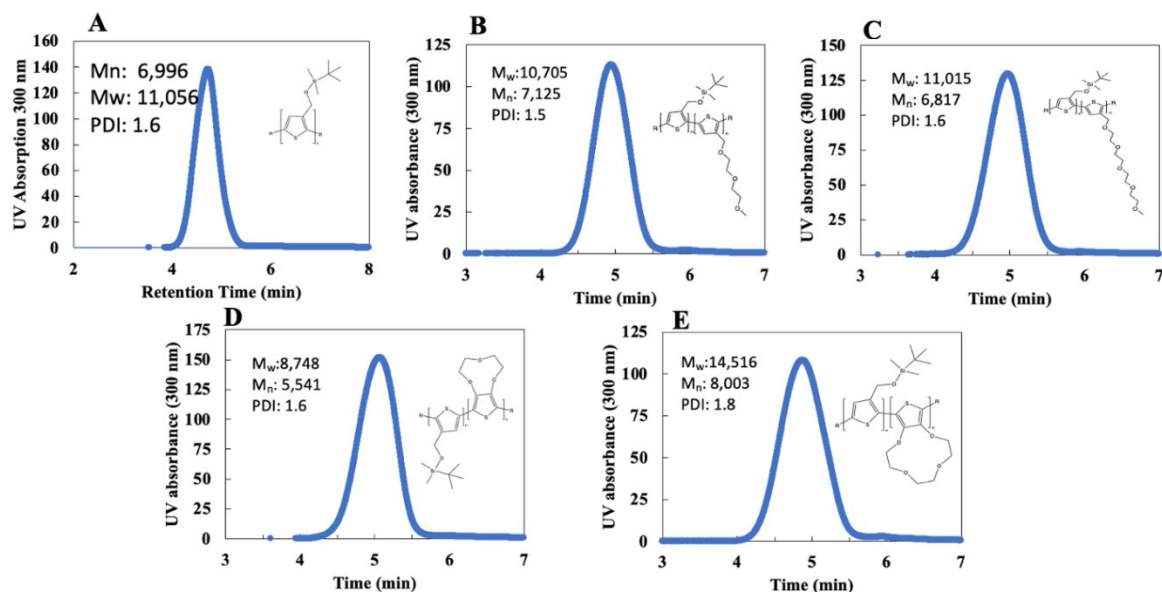


Figure S33. UV SEC trace of A) PTOTBS, B) PTOTBS-co-P3MEEMT, C) PTOTBS-co-P5MEEMT, D) PTOTBS-co-PT3C, and E) PTOTBS-co-PT4C.

We also performed the following morphological characterizations:

Film thickness by optical profilometry: the average thickness of the five homopolymer films was 40-70 nm, and of the six copolymer films, 30-70 nm. None of these are ultrathin on the molecular scale, nor are they thick enough ($>1 \mu\text{m}$) to pose substantial transport barriers or create alternative transport pathways. There was no obvious correlation between thicknesses and vapor responses.

Morphology by AFM: Surface roughness was 0.6-1.2 nm for all eleven polymers of this study; thus, all the polymers were comparably smooth and continuous, making surface morphological features unlikely to be the origins of electronic property and response differences.

Morphology by optical microscopy: the films showed generally similar shallow round granular structures of a few hundreds of μm diameter. PTOH showed some isolated larger grains. None showed obvious pores.

Representative/related homopolymer films were characterized by XRD in a just-published manuscript (Electrochemical Science Advances, <http://doi.org/10.1002/elsa.202100165>, supporting information): P3HT and PTOH characterized in detail in this study, thiophene-4-butyric acid and ester polymers (PT-COOH and PT-COOR) used in a previous study (reference 36) and in the present statistical analysis, and the homopolymer of 3MEEMT, a comonomer of this study. They all showed diffraction peaks at similar positions, except PTOH, which was essentially featureless.

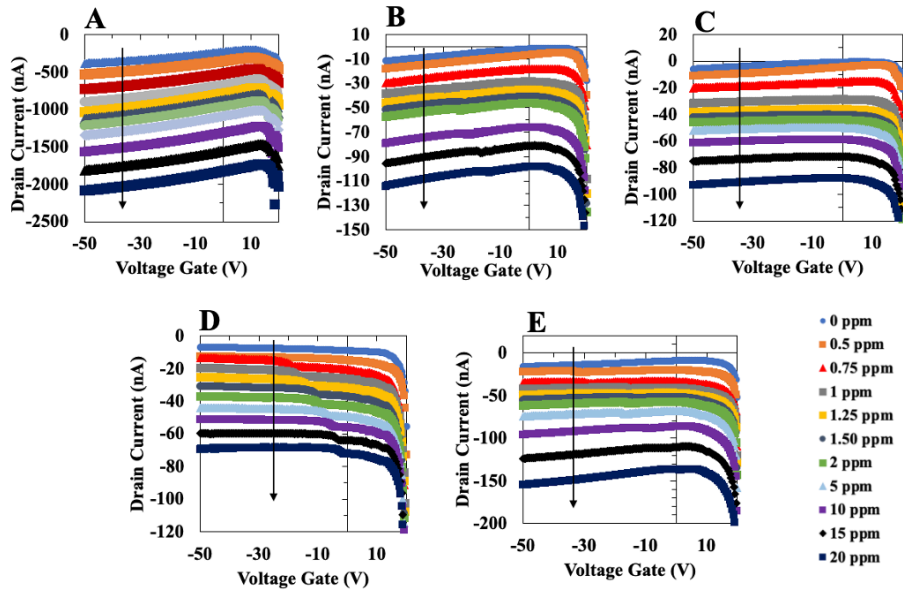


Figure S34. Transfer characteristic for polymer sensing layer A) P3HT-co-PTOH, (B) P3HT-co-P3MEEMT, (C) P3HT-co-P5MEEMT, (D) P3HT-co-PT3C, and (E) P3HT-co-PT4C with continuous exposure to increasing concentrations of NO_2 for 3 minutes before each consecutive measurement.

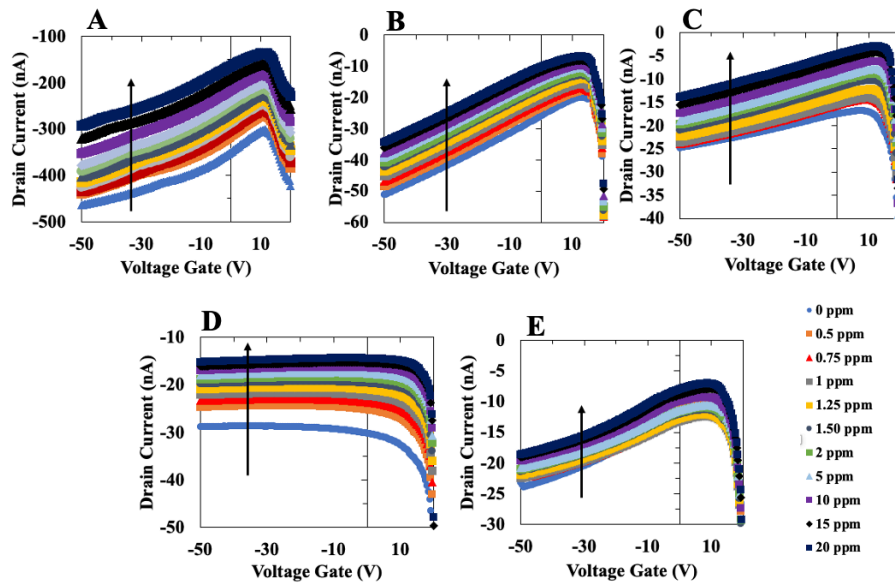


Figure S35. Transfer characteristic for polymer sensing layer A) P3HT-co-PTOH, (B) P3HT-co-P3MEEMT, (C) P3HT-co-P5MEEMT, (D) P3HT-co-PT3C, and (E) P3HT-co-PT4C with continuous exposure to increasing concentrations of NH_3 for 3 minutes before each consecutive measurement.

Figure S36 A-F (Supporting Information) displays the mobility (μ) and threshold voltage (V_{TH}) shift extracted from the transfer curve of each consecutive increasing concentration exposure of NO_2 to each polymer system. They were calculated in the saturation regime ($V_{DS} = -50$ V) by plotting the square root of the drain current versus the gate voltage in the presence of each different vapor (not from the data in Figures 4 and 5). P3HT-co-PTOH displays the highest μ with no gas exposure at $5.36 \times 10^{-4} \text{ cm}^2\text{V}^{-1}\text{s}^{-1}$. P3HT, P3HT-co-P3MEEMT, and P3HT-co-PT4C showed very similar μ at $9.50 \times 10^{-5} \text{ cm}^2\text{V}^{-1}\text{s}^{-1}$, $1.80 \times 10^{-5} \text{ cm}^2\text{V}^{-1}\text{s}^{-1}$, $2.2 \times 10^{-5} \text{ cm}^2\text{V}^{-1}\text{s}^{-1}$, respectively, while P3HT-co-P5MEEMT and P3HT-co-PT3C showed the lowest μ at $8.3 \times 10^{-6} \text{ cm}^2\text{V}^{-1}\text{s}^{-1}$ and $9.2 \times 10^{-6} \text{ cm}^2\text{V}^{-1}\text{s}^{-1}$, respectively. However, the change in μ drastically differs after running through all consecutive increasing NO_2 concentrations. μ increases by 410%, 360%, 730%, 1320%, 820%, and 810% for P3HT, P3HT-co-PTOH, P3HT-co-P3MEEMT, P3HT-co-P5MEEMT, P3HT-co-PT3C, and P3HT-co-PT4C, respectively.

Incorporating a hydroxyl moiety decreases the μ increase from NO_2 exposure compared to P3HT itself while the rest of the oxygen functionalities show μ increases of at least double with that of P5MEEMT increasing 3-fold. The initial threshold voltage is high for P3HT at 14.4 V while P3HT-co-PTOH, P3HT-co-P3MEEMT, P3HT-co-P5MEEMT, P3HT-co-PT3C, and P3HT-co-PT4C are initially at 10, 7.8, 9.2, 11.2, and 9.6 V, respectively. The change in V_{TH} shifts positively (as expected) by a magnitude of 20%, 50%, 60%, 40%, 25%, and 25% for P3HT, P3HT-co-PTOH, P3HT-co-P3MEEMT, P3HT-co-P5MEEMT, P3HT-co-PT3C, and P3HT-co-PT4C, respectively.

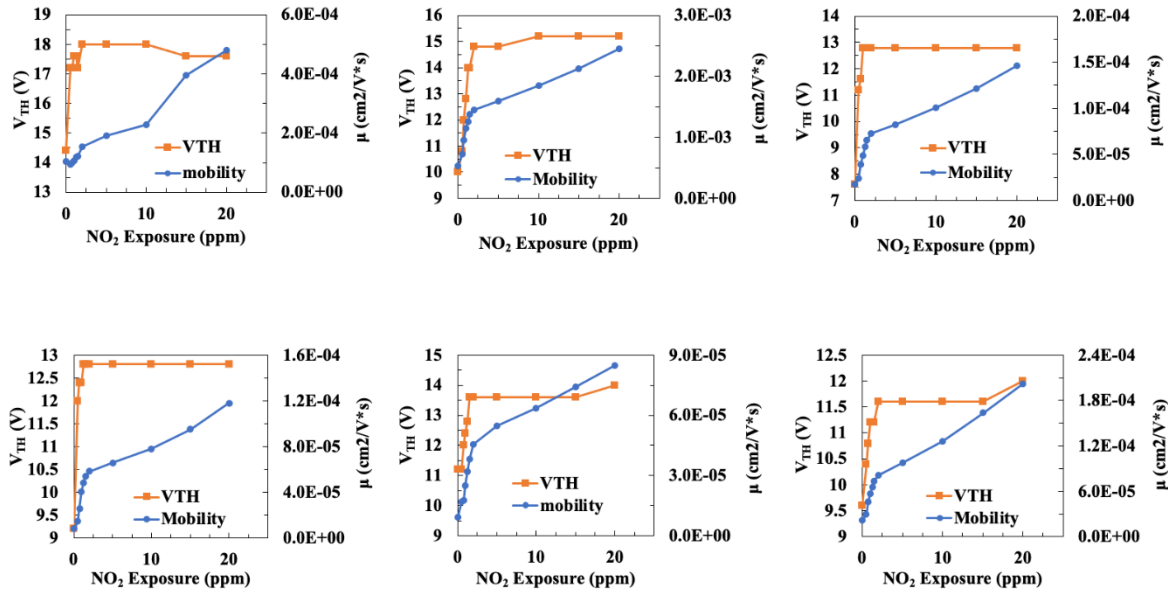


Figure S36. Mobility and Threshold Voltage Shift of A) P3HT, B) P3HT-co-PTOH, C) P3HT-co-P3MEEMT, D) P3HT-co-P5MEEMT, E) P3HT-co-PT3C, and F) P3HT-co-PT4C exposed to NO_2 at consecutive increasing concentrations.

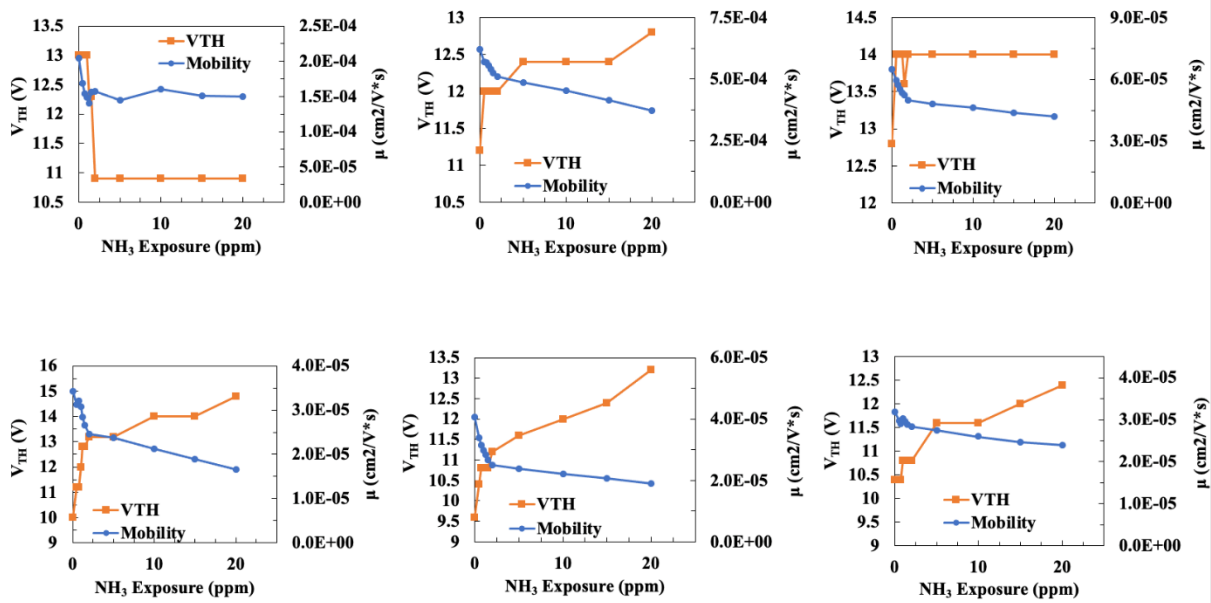


Figure S37. Mobility and Threshold Voltage Shift of A) P3HT, B) P3HT-co-PTOH, C) P3HT-co-P3MEEMT, D) P3HT-co-P5MEEMT, E) P3HT-co-PT3C, and F) P3HT-co-PT4C exposed to NH_3 at consecutive increasing concentrations. μ and V_{TH} shift are extracted from the transfer curve of each consecutive increasing concentration exposure of NH_3 to each polymer system. The change in μ varies slightly after running through all consecutive increasing NH_3 concentrations. The mobility decreases by -30%, -40%, -30%, -50%, -50%, and -25% for P3HT, P3HT-co-PTOH, P3HT-co-P3MEEMT, P3HT-co-P5MEEMT, P3HT-co-PT3C, and P3HT-co-PT4C, respectively.

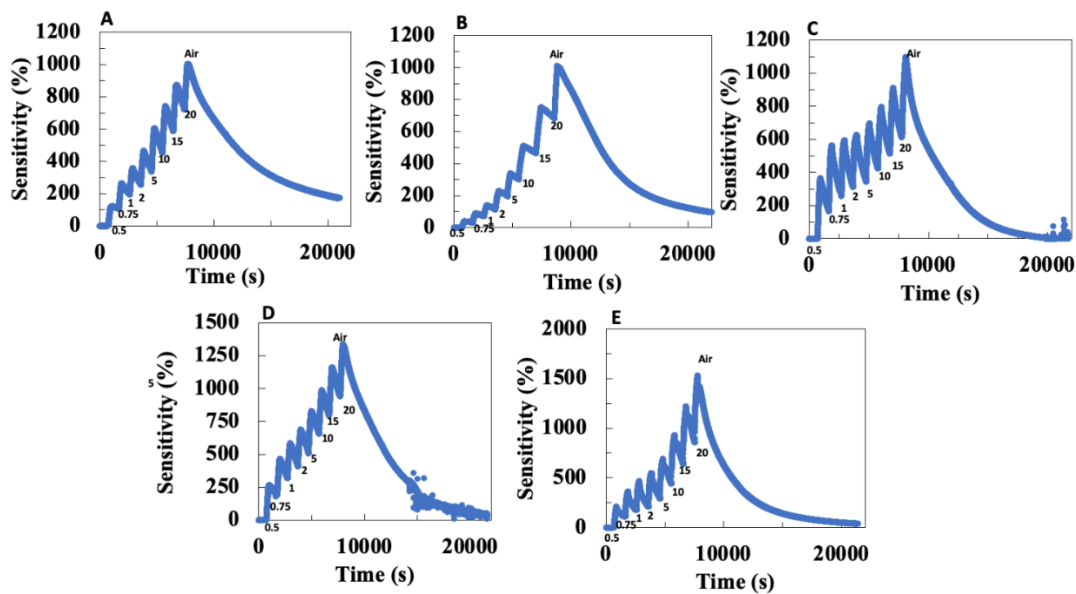


Figure S38. Real time sensitivity and response of A) P3HT-co-PTOH, B) P3HT-co-P3MEEMT, C) P3HT-co-P5MEEMT, D) P3HT-co-PT3C, and E) P3HT-co-PT4C exposed to NO₂ at consecutive increasing concentrations. Small numbers indicate exposure concentration. Total duration of time is 180 seconds followed by 12 minutes of recovery before re-exposure to subsequent higher gas concentration.

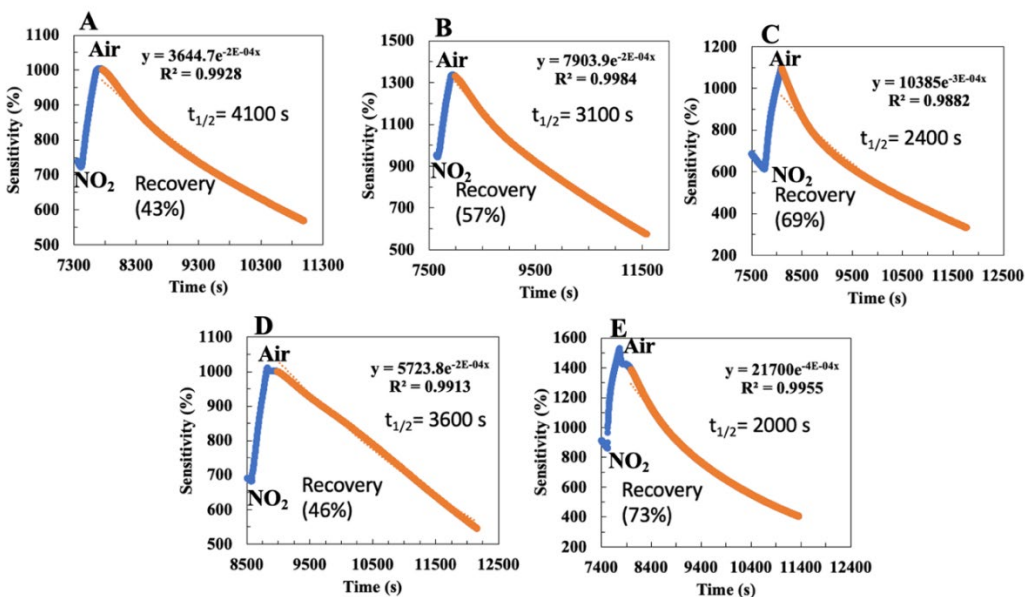


Figure S39. Recovery Analysis of A) P3HT-co-PTOH, B) P3HT-co-P3MEEMT, C) P3HT-co-P5MEEMT, D) P3HT-co-PT3C, and E) P3HT-co-PT4C devices after 20 ppm of NO₂. Best exponential decay fit line obtained with regression being > 98%. Recovery involved sparging continuously with purified air. We fit an exponential line that follows $y=Ae^{kx}$, where x is decay in

seconds (s). A half-life formula was obtained where $t = -\ln(2)/k$. Originally reported in our previous work (reference 36), P3HT had a half-life of 1700 s with a recovery of 67%. In this instance P3HT-co-PTOH, P3HT-co-P3MEEMT, P3HT-co-P5MEEMT, P3HT-co-PT3C, and P3HT-co-PT4C have a half-life of 4100 s, 3100 s, 2400 s, 3600 s, and 2000 s, respectively. The absolute recovery was 43%, 57%, 69%, 46%, and 73%, respectively as well.

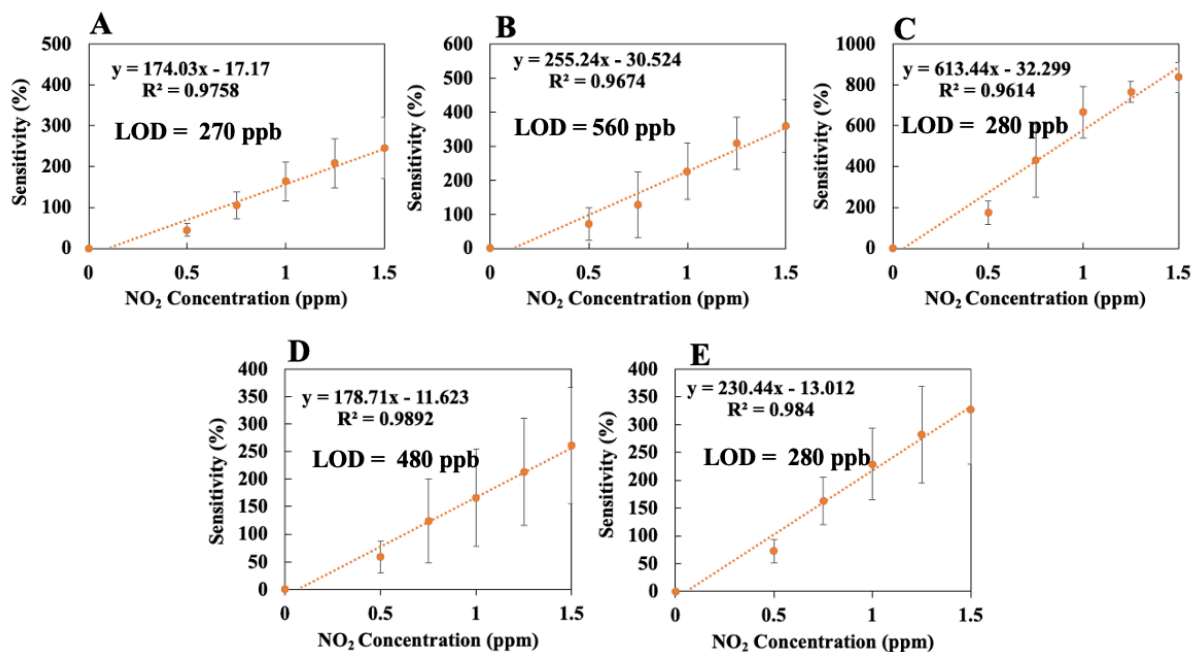


Figure S40. Theoretical extraction of LOD for A) P3HT-co-PTOH, B) P3HT-co-P3MEEMT, C) P3HT-co-P5MEEMT, D) P3HT-co-PT3C, and E) P3HT-co-PT4C exposed to NO_2 at consecutive increasing concentrations at 3 minutes each. Slope represents % / ppm. All polymers displayed a first-order interaction; however, the slope which represents sensitivity (%) per concentration (ppm) appears to significantly increase for P3HT-co-P5MEEMT at 613 % / ppm, while the rest of the polymers display similar slope range of 170 % / ppm, 260 % / ppm, 180 % / ppm, and 230 % / ppm for P3HT-co-PTOH, P3HT-co-P3MEEMT, P3HT-co-PT3C, and P3HT-co-PT4C, respectively. The same principle was used to find the LOD for NH_3 exposure, which was 1.6 ppm, 230 ppb, 320 ppb, 510 ppb and 1.9 ppm which is shown in Supporting Information Figure S41. The limit of detection we reported in our earlier work³⁶ for pristine P3HT was 740 ppb and 639 ppb for NO_2 and NH_3 . The LOD was reduced significantly by incorporating oxygen bearing moieties for each subset of copolymers compared to pristine P3HT for NO_2 exposure. However, for NH_3 exposure, incorporating oxygen functional moieties such as PTOH and PT4C resulted in increasing the LOD to the parts per million (ppm) regime. However, the rest of the copolymers displayed a decrease in LOD suggesting that the interaction towards NH_3 must be stronger.

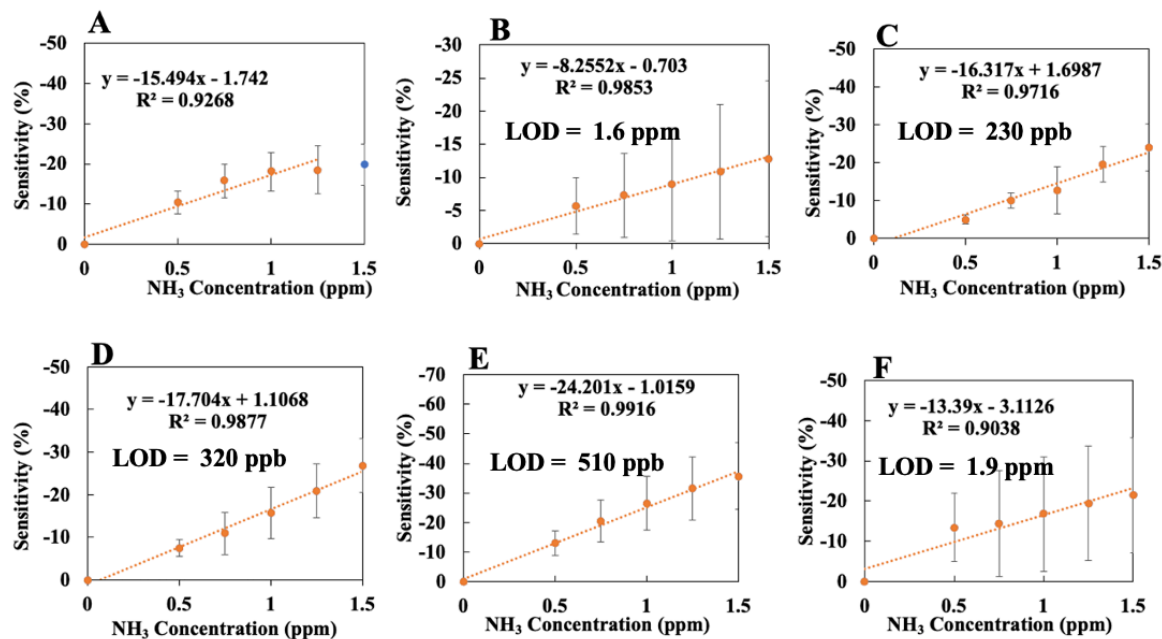


Figure S41. Theoretical extraction of LOD for A) P3HT, B) P3HT-co-PTOH, C) P3HT-co-P3MEEMT, D) P3HT-co-P5MEEMT, E) P3HT-co-PT3C, and F) P3HT-co-PT4C exposed to NH_3 at consecutive increasing concentrations at 3 minutes each. Slope represents % / ppm.

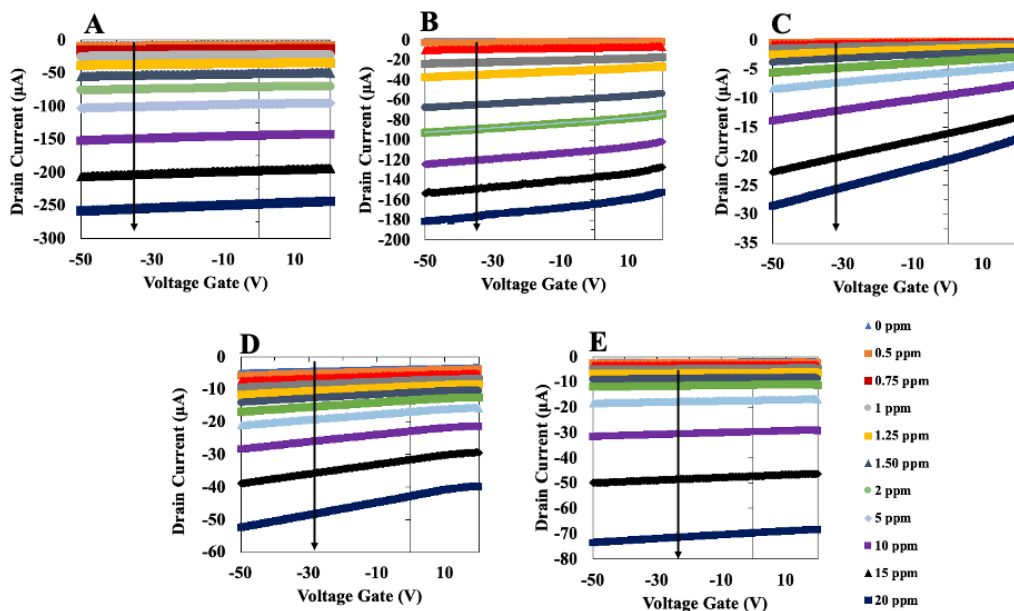


Figure S42. Transfer characteristic for polymer sensing layer A) PTOH, (B) PTOH-co-P3MEEMT, (C) PTOH-co-P5MEEMT, (D) PTOH-co-PT3C, and (E) PTOH-co-PT4C with continuous exposure to increasing concentrations of NO_2 for 3 minutes before each consecutive measurement.

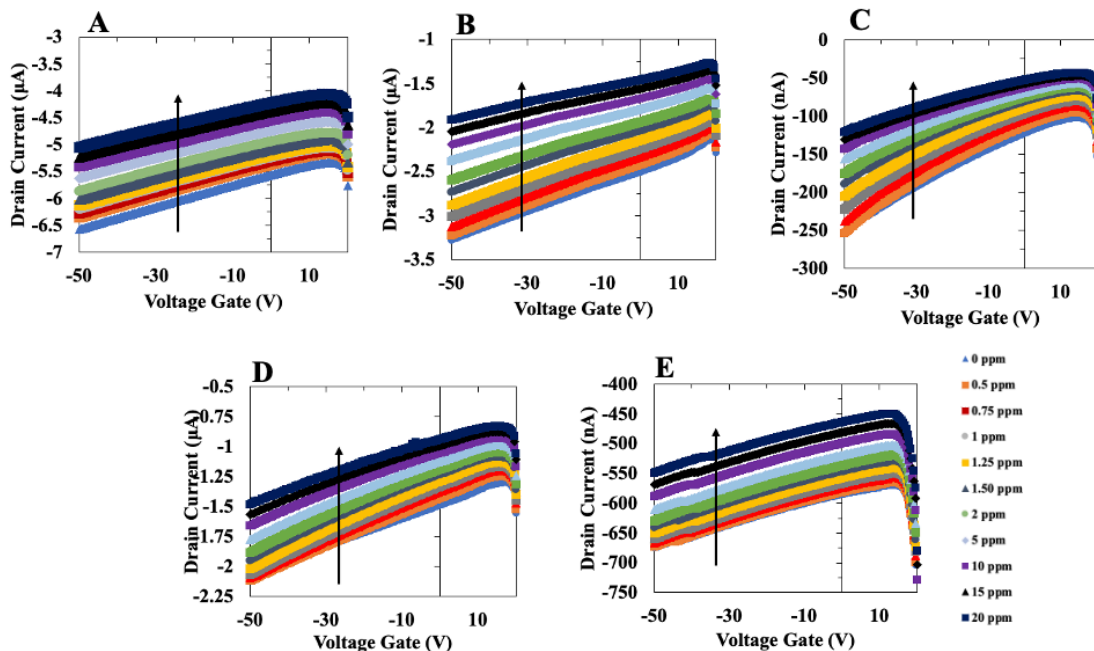


Figure S43. Transfer characteristic for polymer sensing layer A) PTOH, (B) PTOH-co-P3MEEMT, (C) PTOH-co-P5MEEMT, (D) PTOH-co-PT3C, and (E) PTOH-co-PT4C with continuous exposure to increasing concentrations of NH_3 for 3 minutes before each consecutive measurement.

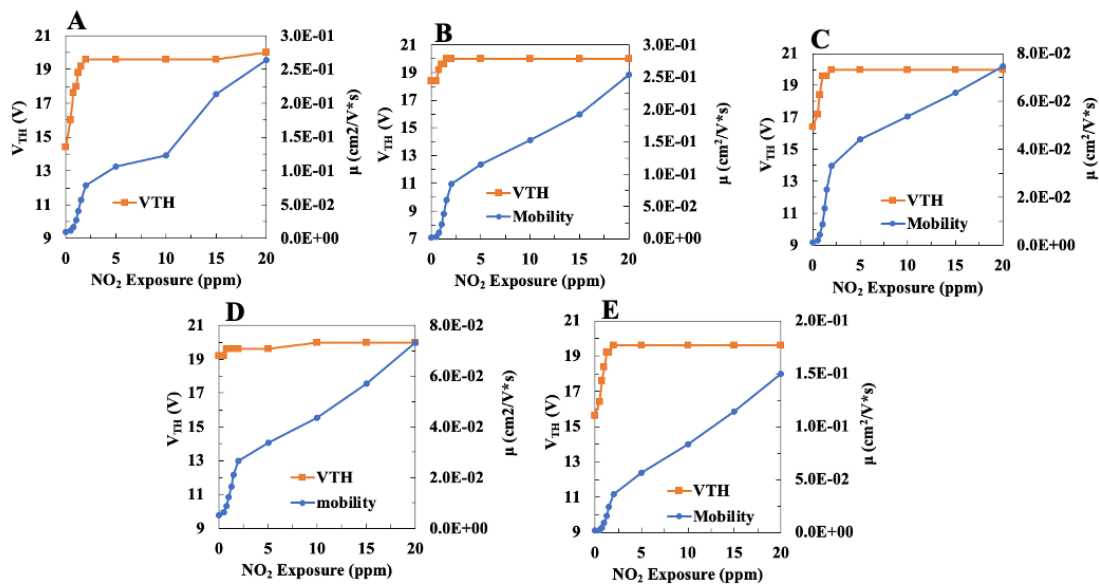


Figure S44. Mobility and Threshold Voltage Shift of A) PTOH, B) PTOH-co-P3MEEMT, C) PTOH-co-P5MEEMT, D) PTOH-co-PT3C, and E) PTOH-co-PT4C exposed to NO_2 at consecutive increasing concentrations.

PTOH-co-P3MEEMT, PTOH-co-P5MEEMT, PTOH-co-PTOH-PT3C and PTOH-co-PT4C displayed slightly lower μ at $3.40 \times 10^{-3} \text{ cm}^2\text{V}^{-1}\text{s}^{-1}$, $1.20 \times 10^{-3} \text{ cm}^2\text{V}^{-1}\text{s}^{-1}$, $5.30 \times 10^{-3} \text{ cm}^2\text{V}^{-1}\text{s}^{-1}$ and $2.50 \times 10^{-3} \text{ cm}^2\text{V}^{-1}\text{s}^{-1}$, respectively. PTOH, PTOH-co-P3MEEMT, PTOH-co-P5MEEMT, PTOH-co-PTOH-PT3C and PTOH-co-PT4C all demonstrated exceedingly large change in μ with exposure to NO_2 : 2200%, 7400%, 6200%, 1300%, and 5800%, respectively. PTOH-co-P3MEEMT, PTOH-P5MEEMT, and PTOH-co-PT4C displayed a much larger μ change compared to PTOH itself, while PTOH-co-PT3C displayed the smallest change and less than PTOH itself. Incorporating oxygen functionalities such as P3MEEMT, P5MEEMT, and PT4C results in an increase in μ from NO_2 exposure by at least 3-fold, while incorporating PT3C decreases μ enhancement from NO_2 exposure by half.

In Figure S45, the change in μ differs slightly after running through all consecutive increasing NH_3 concentrations. μ decreases by -21%, -38%, -50%, -19%, and -17% for PTOH, PTOH-co-P3MEEMT, PTOH-co-P5MEEMT, PTOH-co-PT3C, and PTOH-co-PT4C, respectively.

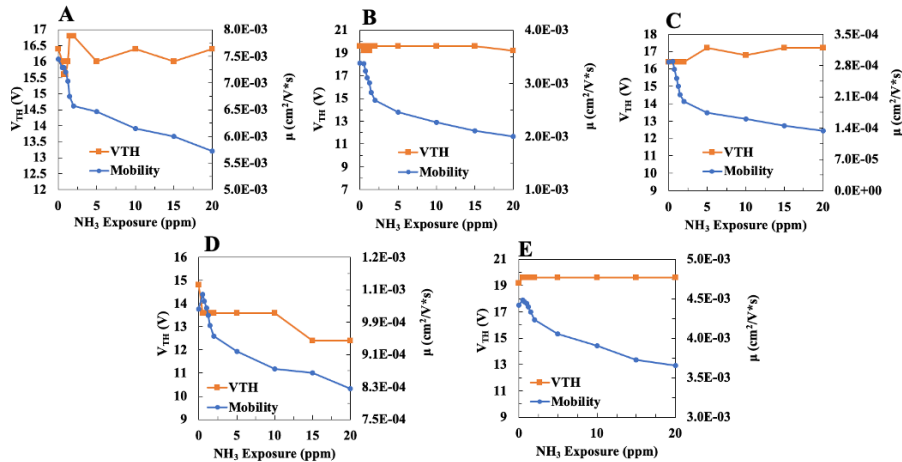


Figure S45. Mobility and Threshold Voltage Shift of A) PTOH, B) PTOH-co-P3MEEMT, C) PTOH-co-P5MEEMT, D) PTOH-co-PT3C, and E) PTOH-co-PT4C exposed to NH₃ at consecutive increasing concentrations.

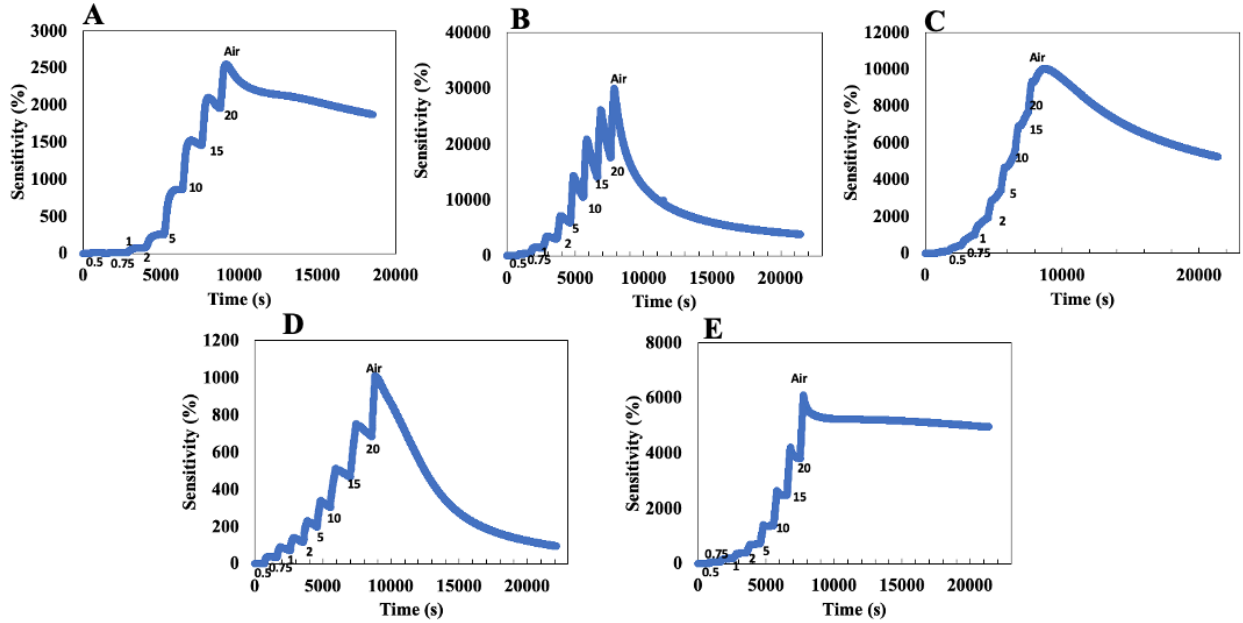


Figure S46. Real time sensitivity and response of A) PTOH, B) PTOH-co-P3MEEMT, C) PTOH-co-P5MEEMT, D) PTOH-co-PT3C, and E) PTOH-co-PT4C exposed to NO₂ at consecutive increasing concentrations. Small numbers indicate concentration exposure amount. Total duration of time is 180 seconds followed by 12 minutes of recovery before re-exposure to subsequent higher gas concentration.

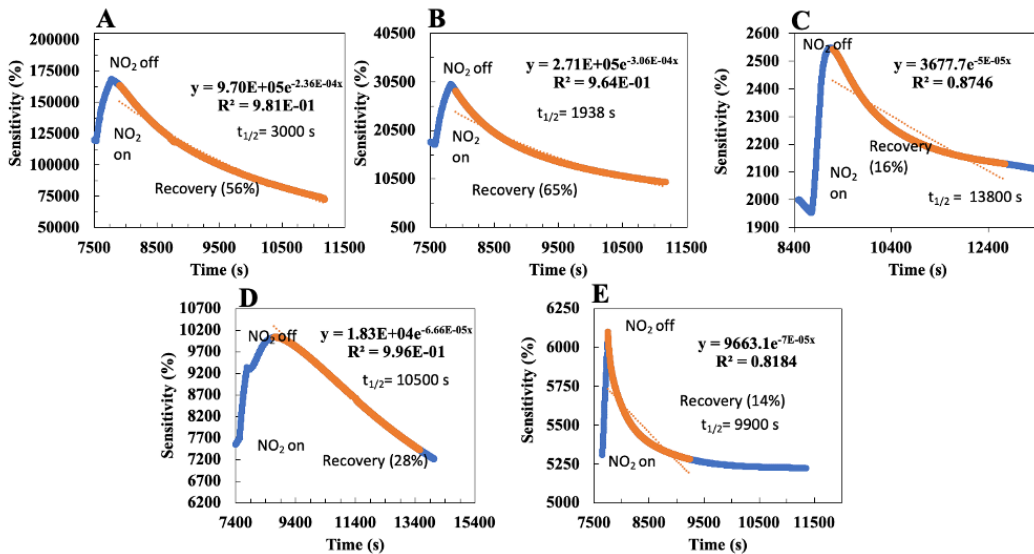


Figure S47. Recovery Analysis of A) PTOH, B) PTOH-co-P3MEEMT, C) PTOH-co-P5MEEMT, D) PTOH-co-PT3C, and E) PTOH-co-PT4C devices after 20 ppm of NO₂. Best exponential decay fit line obtained with regression being > 98%. Recovery involved sparging continuously with purified air. Half-life formula obtained where $t = -\ln(2)/k$. Recovery of PTOH, PTOH-co-P3MEEMT, PTOH-co-P5MEEMT, PTOH-co-PT3C, and PTOH-co-PT4C has a half-life of 3000 s, 1900 s, 13,800 s, 10,500 s, and 9,900 s, respectively. The absolute recovery was 56%, 65%, 16%, 28%, and 14%, respectively as well. This suggests that the oxygen bearing functional groups lead to sluggish recovery under ambient conditions. PTOH alone or a copolymer with a shorter chain (P3MEEMT) shows relatively manageable recovery rates, however, increasing the glycol chain length or incorporating oxygen bearing functionalities that generate cavities impedes the recovery. These results are different from those from P3HT based copolymers, indicating that there is an enhanced synergistic interaction between PTOH and its copolymers that results in greater binding of NO₂.

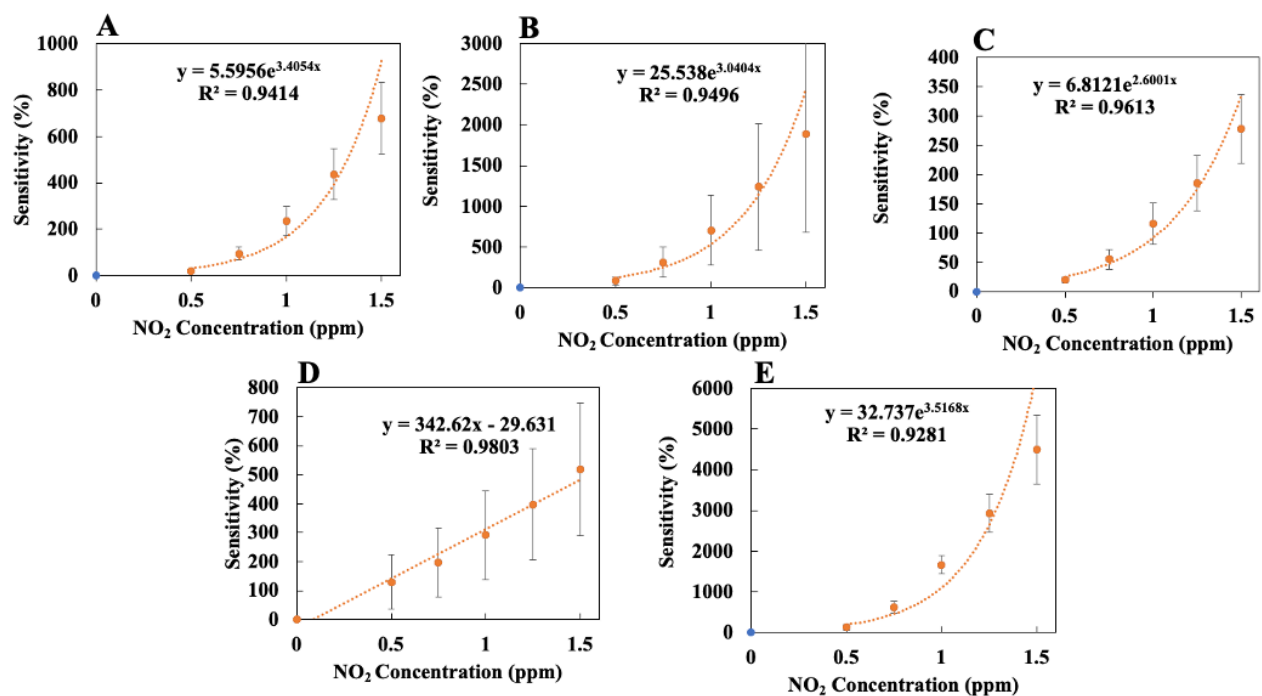


Figure S48. Theoretical extraction of LOD for A) PTOH, B) PTOH-co-P3MEEMT, C) PTOH-co-P5MEEMT, D) PTOH-co-PT3C, and E) PTOH-co-PT4C exposed to NO₂ at consecutive increasing concentrations at 3 minutes each. Slope represents % / ppm.

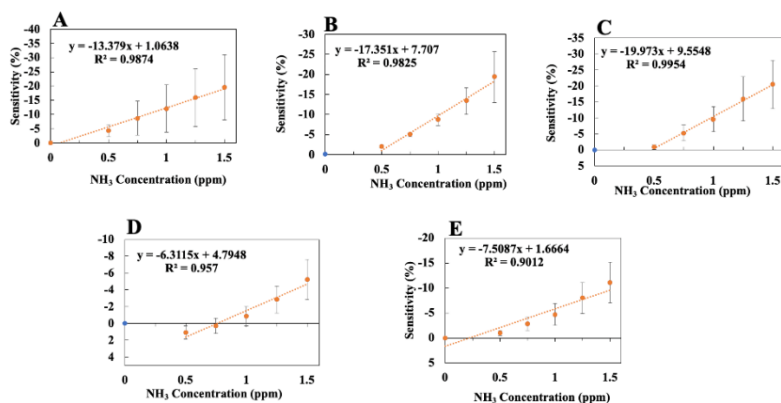


Figure S49. Theoretical extraction of LOD for A) PTOH, B) PTOH-co-P3MEEMT, C) PTOH-co-P5MEEMT, D) PTOH-co-PT3C, and E) PTOH-co-PT4C exposed to NH₃ at consecutive increasing concentrations at 3 minutes each. Slope represents % / ppm.

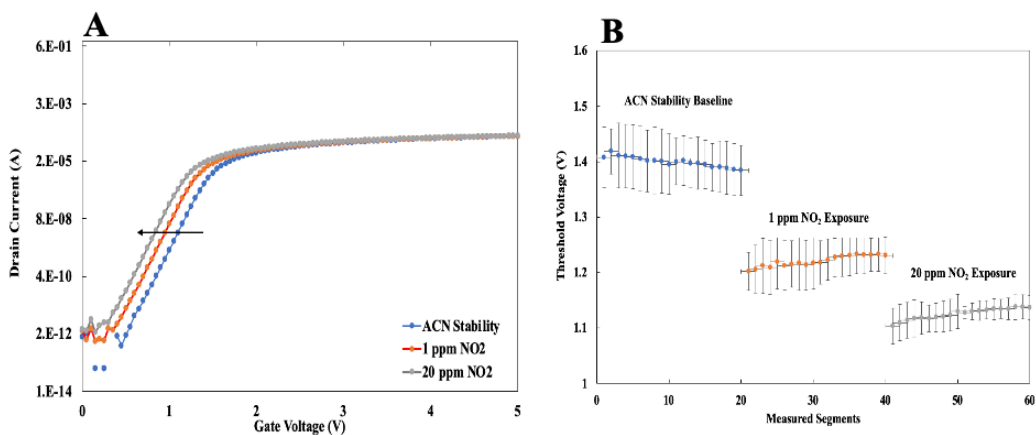


Figure S50. A) Transfer curve of remote-gate field effect transistor for PTOH with NO₂ exposure for 20 minutes at 1 ppm and 20 ppm. Acetonitrile was used as the contact solvent between extended gate and remote gate field effect transistor. V_{TH} analysis of PTOH with exposure to NO₂ (1 ppm and 20 ppm) using ACN as contact solvent is seen in B). Segment measurements pertain to 20 consecutive scans that are averaged with 4 sample trials of each sample measurement. Plots show initial drift under acetonitrile and shifts from NO₂ exposure followed by reapplication of acetonitrile.

Sample	Gas	Concentration	σ (S/cm)	$\Delta V_{TH, RG}$ (V)	P (cm ⁻³) : RG	μ (cm ² /V*s) : RG
PTOH	-	No Exposure	5.90E-04 ± 1.1E-04	-	5.80E17 ± 1.80E17	6.90E-03 ± 3.0E-3
	NO ₂	1 ppm	5.50E-02 ± 2.0E-02	-0.18 ± 0.01	6.10E20 ± 1.9E20	6.4E-02 ± 2.0E-2
	NH ₃	1 ppm	2.30E-02 ± 9.3E-03	N/A	N/A	N/A

Table S1. Electrical parameters consisting of conductivity, $\Delta V_{TH, RG}$, hole concentration of PTOH before and after 1 ppm exposure of NO₂ due to calculating the voltage shift with the incorporation of the RG FET platform. $\Delta V_{TH, RG}$ was calculated by taking the average of $V_{TH, RG}$ from 4 trials. Mobility for unexposed devices was obtained from FET measurement, while mobility for NO₂-exposed devices was calculated based on hole concentrations obtained by using $\sigma = e \cdot \mu_h \cdot p_0$. Initial hole concentration was obtained from OFET μ_h using transfer curve and conductivity (σ).

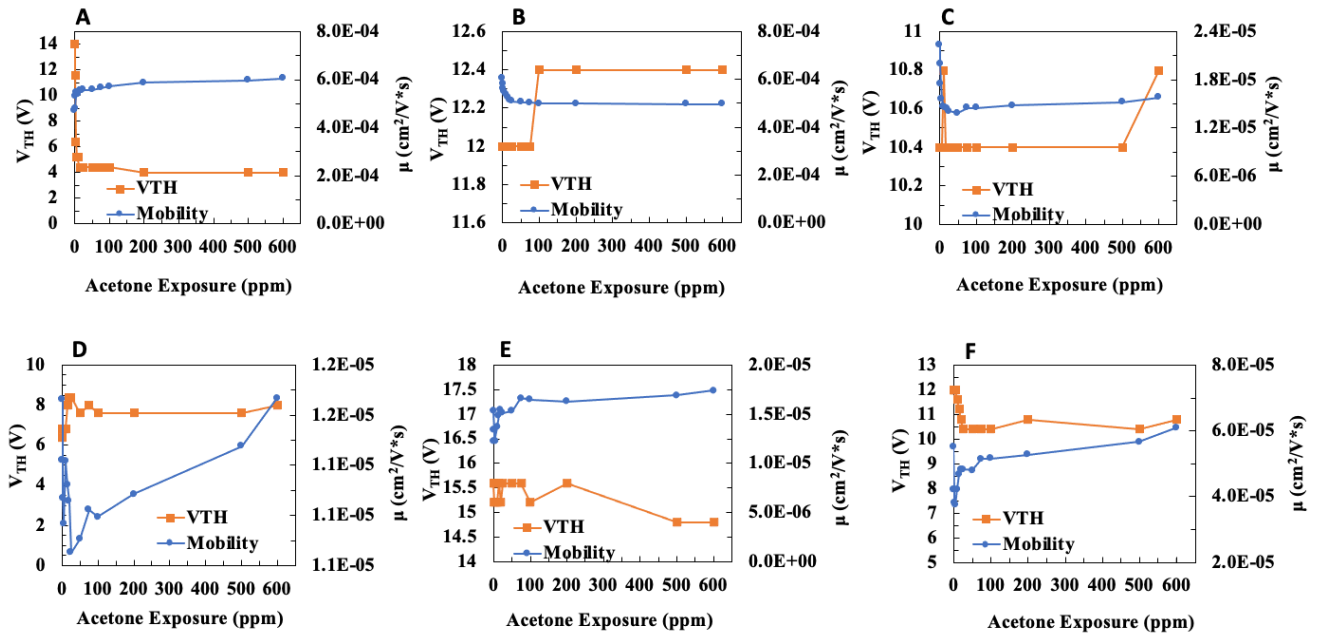


Figure S51. Mobility and Threshold Voltage Shift of A) P3HT, B) P3HT-co-PTOH, C) P3HT-co-P3MEEMT, D) P3HT-co-P5MEEMT, E) P3HT-co-PT3C, and F) P3HT-co-PT4C exposed to acetone at consecutive increasing concentrations.

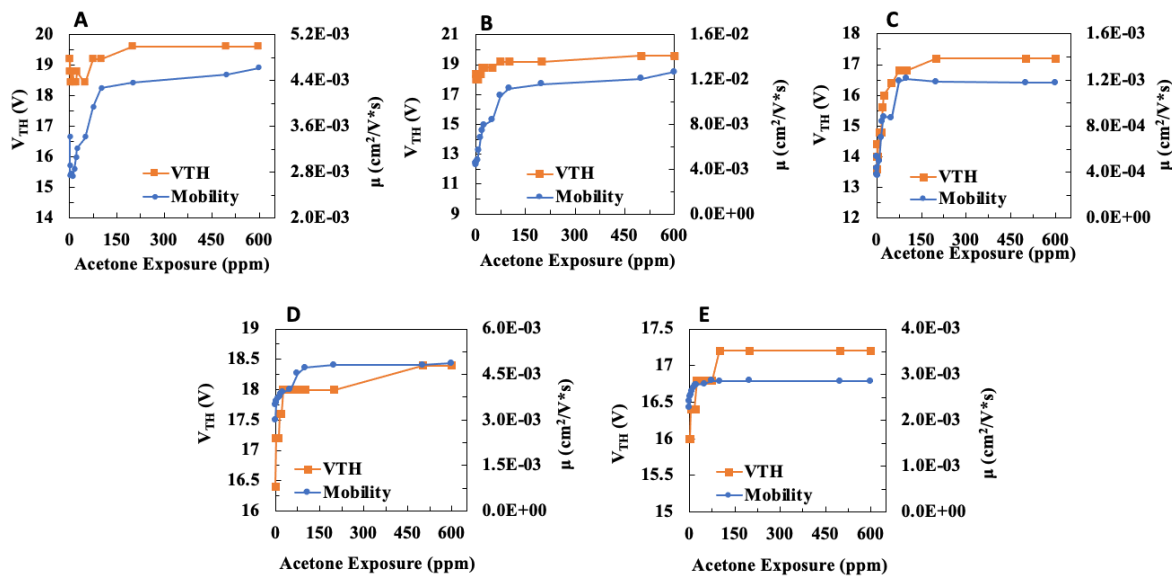


Figure S52. Mobility and Threshold Voltage Shift of A) PTOH, B) PTOH-co-P3MEEMT, C) PTOH-co-P5MEEMT, D) PTOH-co-PT3C, and E) PTOH-co-PT4C exposed to acetone at consecutive increasing concentrations.

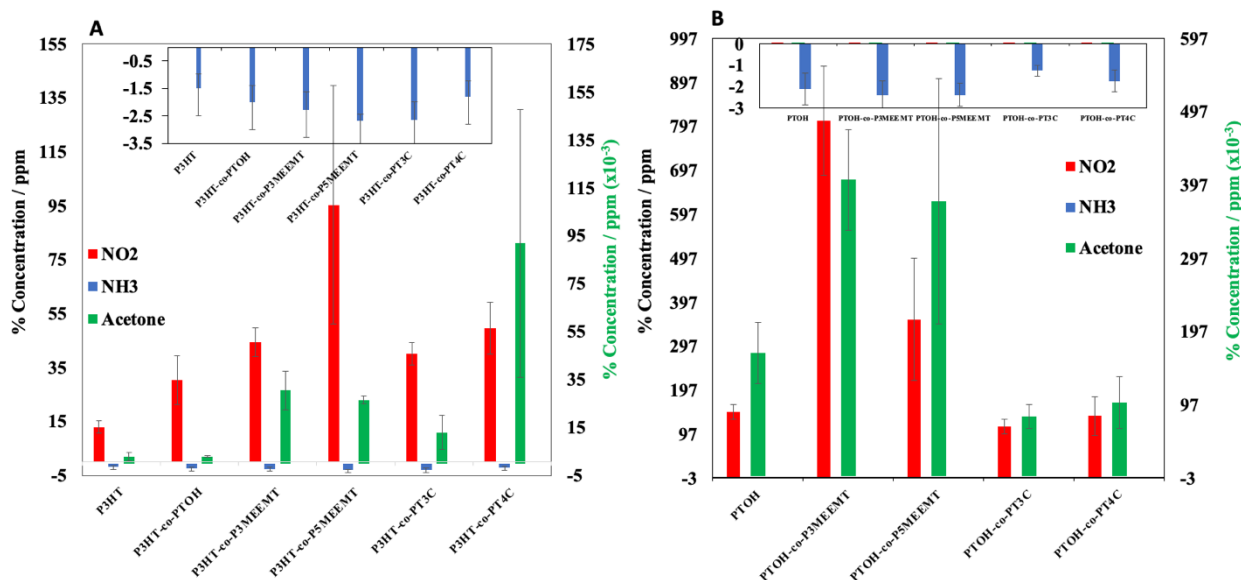


Figure S53. Cumulative summary of gas sensitivity of A) P3HT and P3HT-copolymers and B) PTOH and PTOH-copolymers that is normalized using gas concentration of %/ppm for rational comparison of sensing performance.